Thermal conductivity and radiogenic heat production of sedimentary and magmatic rocks in the Northeast German Basin

Ben Norden and Andrea Förster

ABSTRACT

Thermal rock properties were determined for the Northeast German Basin, a subbasin of the southern Permian basin in Europe. The new thermal data provide new aspects for the determination of heat flow and for hydrocarbon and geothermal resource evaluation in the basin. Thermal conductivity was measured on drill-core samples using the optical scanning method. Values for Permian and pre-Permian clastic rocks are variable (2.3–4.8 W/m/K) because of different depositional environments, compaction, and cementation reflected in lithology. Permian–Carboniferous igneous rocks show lowest thermal conductivity in basalts (2.2 W/m/K) and highest (3.1 W/m/K) in granitoids. Anisotropy of thermal conductivity in all rocks is low. Formation thermal conductivity was determined by upscaling the values determined for single lithotypes. Radiogenic heat production was determined on drill cores for the upper Paleozoic sediments and igneous rocks. For the younger formations without sample control, a well-log approach was used. The heat production of sedimentary rocks is lowest (0.4 $\mu W/m^3$) in the Permian (Zechstein) salt and anhydrite and highest (2.1 $\mu W/m^3$) in the Permian (Rotliegende) clastic rocks. Heat production of the Permian–Carboniferous rhyolites and granitoids is on the order of 2.6–3.8 $\mu W/m^3$, and heat production of andesites and basaltoids is on the order of 0.9–1.9 and 0.1–0.7 $\mu W/m^3$, respectively. The contribution to surface heat flow by these up to 2-km (1.2-mi)-thick igneous complexes amounts to 7 mW/m^2 at a maximum. On the same order is the total heat budget provided by the supra-Permian sedimentary succession in the basin.

Manuscript received June 9, 2005; provisional acceptance September 30, 2005; revised manuscript received January 3, 2006; final acceptance January 25, 2006.
DOI:10.1306/01250605100

AUTHORS

BEN NORDEN ~ *GeoForschungsZentrum Potsdam, Telegrafenberg, 14473 Potsdam, Germany; norden@gfz-potsdam.de*

Ben Norden received a degree in geology (diploma) from the University of Hamburg in 1999. Since 2000, he has worked at the GeoForschungsZentrum Potsdam. He received a master's degree in engineering from the University of Applied Sciences, Cologne, in 2003 and a Ph.D. in geosciences from the Freie Universität, Berlin, in 2004. Norden is currently working on a CO_2 storage project. His research interests include heat flow and fluid flow.

ANDREA FÖRSTER ~ *GeoForschungsZentrum Potsdam, Telegrafenberg, 14473 Potsdam, Germany*

Andrea Förster is a staff scientist at the GeoForschungsZentrum Potsdam, Germany. She received a diploma degree in geology, a Ph.D., and a Habilitation degree from the Ernst-Moritz-Arndt-Universität, Greifswald, Germany. Her current research involves the analysis of the earth thermal field, the determination of heat flow, and explorational aspects of applied geothermics. She is also engaged in research focused on the storage of carbon dioxide in saline aquifers.

ACKNOWLEDGEMENTS

The EEG Erdöl Erdgas GmbH (Berlin) is thanked for providing parts of the industrial borehole data. The geological surveys Landesamt für Bergbau, Geologie und Rohstoffe Brandenburg (Cottbus/Kleinmachnow); Landesamt für Umwelt, Naturschutz und Geologie Mecklenburg-Vorpommern (Schwerin); and Geologisches Landesamt Sachsen-Anhalt (Halle) are acknowledged for the supply of borehole information and for the support of the core sampling. The thermal conductivity of a subset of samples was measured at the Institut für Geowissenschaftliche Gemeinschaftsaufgaben (Hannover) using the optical-scanning apparatus supervised by R. Schellschmidt. S. Fricke (Gesellschaft, für Bohrlochmessungen, Gommern), which provided basic information concerning gamma-ray recordings in non-API units. R. Naumann and P. Dulski (GeoForschungsZentrum Potsdam) are thanked for performing the geochemical analyses. The article benefited from valuable comments of H.-J. Förster (University of Potsdam) on an earlier version. The authors are indebted to the AAPG referees for their thought-provoking comments and valuable suggestions.

DATASHARE 21

Tables A1–A5 are accessible in an electronic version on the AAPG Web site as Datashare 21 at <www.aapg.org/datashare/index.html>.

INTRODUCTION

In recent years, the Northeast German Basin (NEGB) has been the target of multifaceted geoscientific research. Seismic, magnetic, and gravimetric investigations were aimed at the interpretation of the geodynamic origin of the basin in the late Carboniferous, its post-Permian structural modification, and its geometry and composition in a global realm. Embedded in this framework were studies that focused on the generation and migration of hydrocarbons and the use of the basin's geothermal potential for district heating and generation of electrical power. All previous studies relied on knowledge of the physical properties of the rocks comprising the sedimentary fill of the basin and the basement. However, despite numerous efforts made in the past to model the basin, no in-depth investigations of the rock properties involved were made. This article fills this gap in knowledge by reporting for the first time measured values of thermal properties (thermal conductivity and radiogenic heat production) attributed to lithology and stratigraphy.

The thermal conductivity of rocks is one of the major factors that affect temperatures in sedimentary basins and, therefore, should be addressed in basin analysis. Blackwell and Steele (1989) describe this effect on the temperature distribution to be significant (on the order of 50–100%). As a result of different thermal conductivity, the thermal structure of a basin may change laterally and vertically even if the heat flow into the basin is regionally the same. Although there is consensus about the importance of thermal conductivity in basin studies, little work has been done in measuring this parameter at basinwide scales. In this article, thermal conductivity was determined in the NEGB for single lithotypes and geologic formations of upper Paleozoic age, which formed the target of several decades of hydrocarbon exploration. This study investigated whether rocks of the same stratigraphic unit, but from different regions in the basin, have significantly different thermal conductivity.

In contrast to the thermal conductivity, the radiogenic heat production has a second-order effect on the temperature distribution (20–50%; Blackwell and Steele, 1989). However, the importance of radiogenic heat production becomes evident in heat-flow studies and the modeling of deep sedimentary basins (e.g., Deming et al., 1990, and references therein). Changes in radiogenic heat production of the underlying basement cause heat-flow variations within a sedimentary basin, which, in turn, change the temperature in direct proportion to the heat-flow variations. Prior to this study, no data on radiogenic heat production were available for the NEGB. Thus, it was timely to determine this parameter for lithotypes and geologic formations and to quantify the heat budget of thick volcanic series and of the sedimentary succession in the basin.

In conjunction with previously analyzed borehole temperature data (Förster, 2001), the thermal data of this article constitute the basis for the determination and interpretation of the surface heat flow in the NEGB (B. Norden, 2005, unpublished data). In addition, the new data alter thermal-maturation models of the basin. Although the study briefly quantifies expected changes, a comprehensive maturation study, however, is beyond the scope of this article.

The experiences and data reported here may also be useful for future thermal studies in neighboring basins of similar geology.

GEOLOGICAL SETTING

The NEGB is a subbasin of the southern Permian Basin in Europe (Ziegler, 1990; Glennie, 1998) extending from the middle of England to Poland (Figure 1). To the west, the NEGB is connected with the Northwest German Basin. The NEGB is bordered on the north by the Tornquist–Teisseyre zone and the Caledonian deformation front and on the south by the Elbe Line. The basin initiation started after the main consolidation of central Europe, which occurred in the Devonian to Carboniferous and is known as the Variscan orogeny.

Permian rocks in the basin are underlain by a basement of variable composition and age. The basement is subdivided into the Variscan-age fold and thrust zone (folded rocks of pre-Permian age) in the south and the Variscan-age foreland basin (unfolded pre-Permian rocks) in the north (Figure 2). In the latter, Carboniferous and Devonian rocks discordantly overlie basement units that were either folded during the Caledonian orogeny (northern part) or consolidated in earlier times (southern part).

Tectonic movements in the late Carboniferous have caused activation of fault systems associated with the emplacement of up to 2000-m (6600-ft)-thick Permian–Carboniferous volcanic series (Figure 2) in pull-apart basins (Benek et al., 1996). These volcanic rocks comprise 70% rhyolites (including ignimbrites), 26% andesites, and about 4% basalts (including dolerites) (R. Benek, 1995, personal communication). The

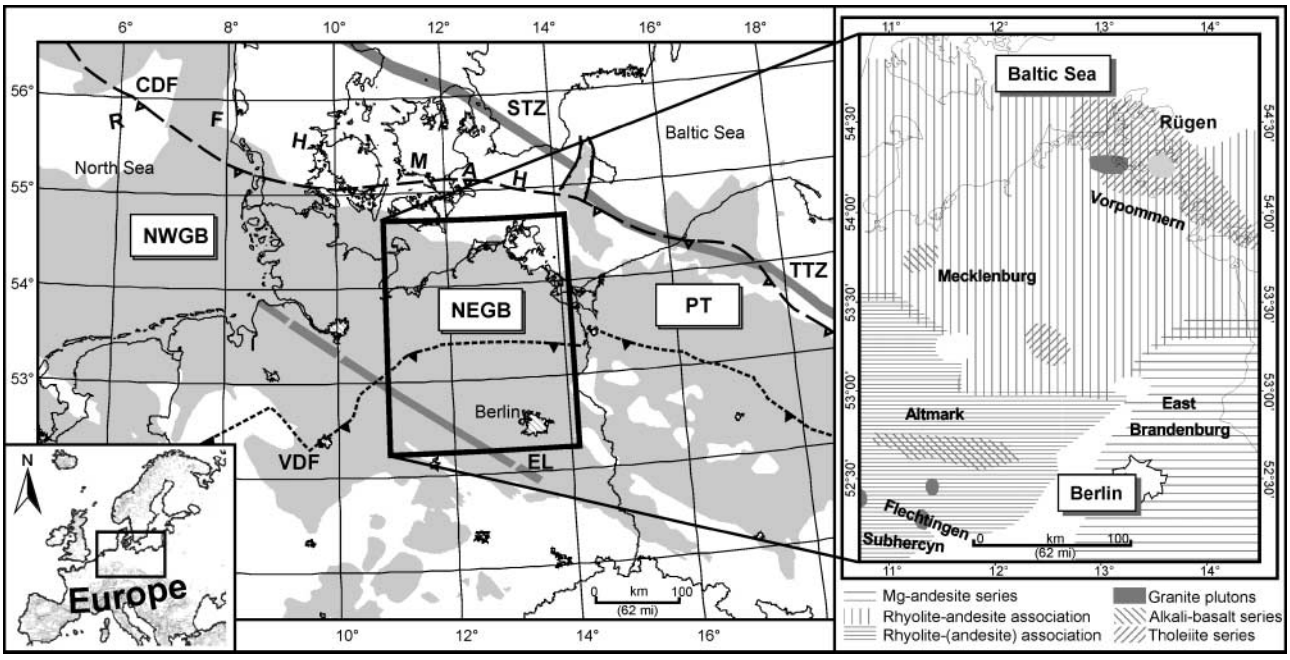

Figure 1. Location of the Northeast German Basin (NEGB) as part of the mid-European basin system with inset map showing the Permian–Carboniferous magmatic provinces: Mecklenburg Vorpommern, Rügen, Altmark Flechtingen Subhercyn, and East Brandenburg. Gray area shows the distribution of Rotliegende sediments. NWGB = Northwest German Basin; PT = Polish trough; EL = Elbe Line; STZ = Sorgenfrey–Tornquist zone; TTZ = Theisseire–Tornquist zone; RFH = Rynkøbing-Fyn high; MAH = Møn-Arkona high; CDF = Caledonian deformation front; VDF = Variscan deformation front (modified from Ziegler, 1990; Benek et al., 1996; Lokhorst, 1998; Scheck and Bayer, 1999).

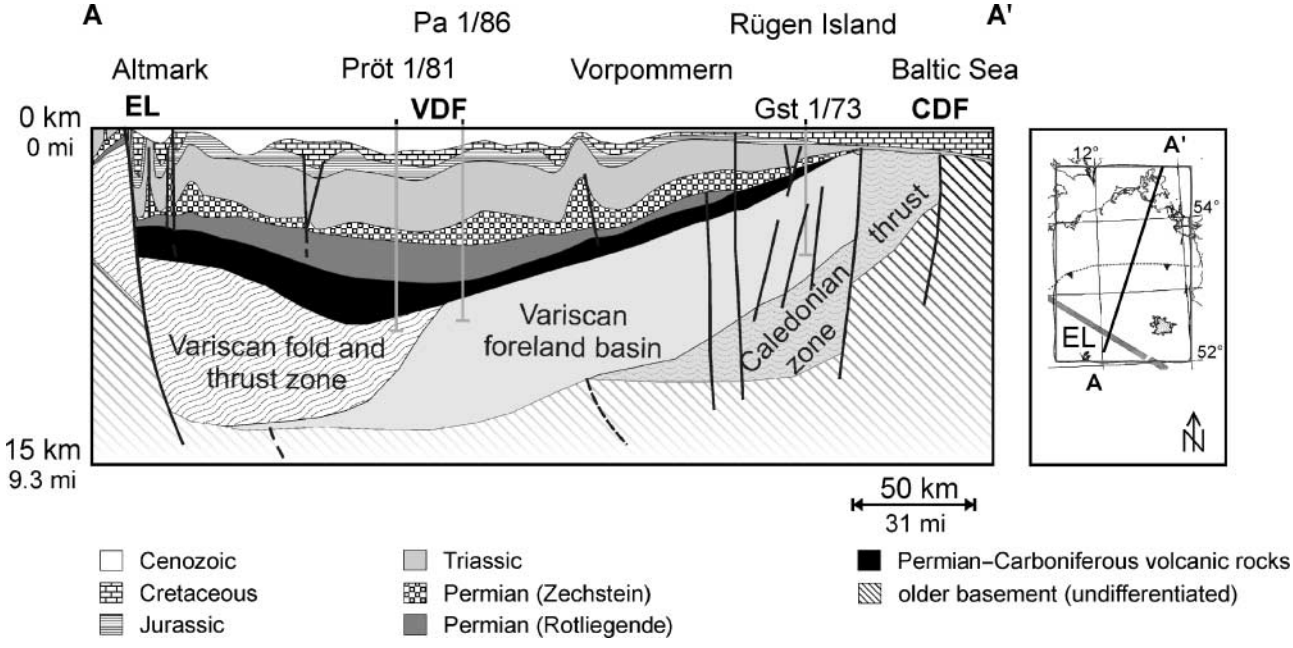

Figure 2. Schematic cross section of the Northeast German Basin (NEGB) (modified from Franke et al., 1996). The tectonically relative undisturbed Rotliegende succession is overlain by highly deformed post-Rotliegende sediments. Note the Zechstein salt domes. Vertical exaggeration = approximately 24-fold. For abbreviations, see Figure 1.

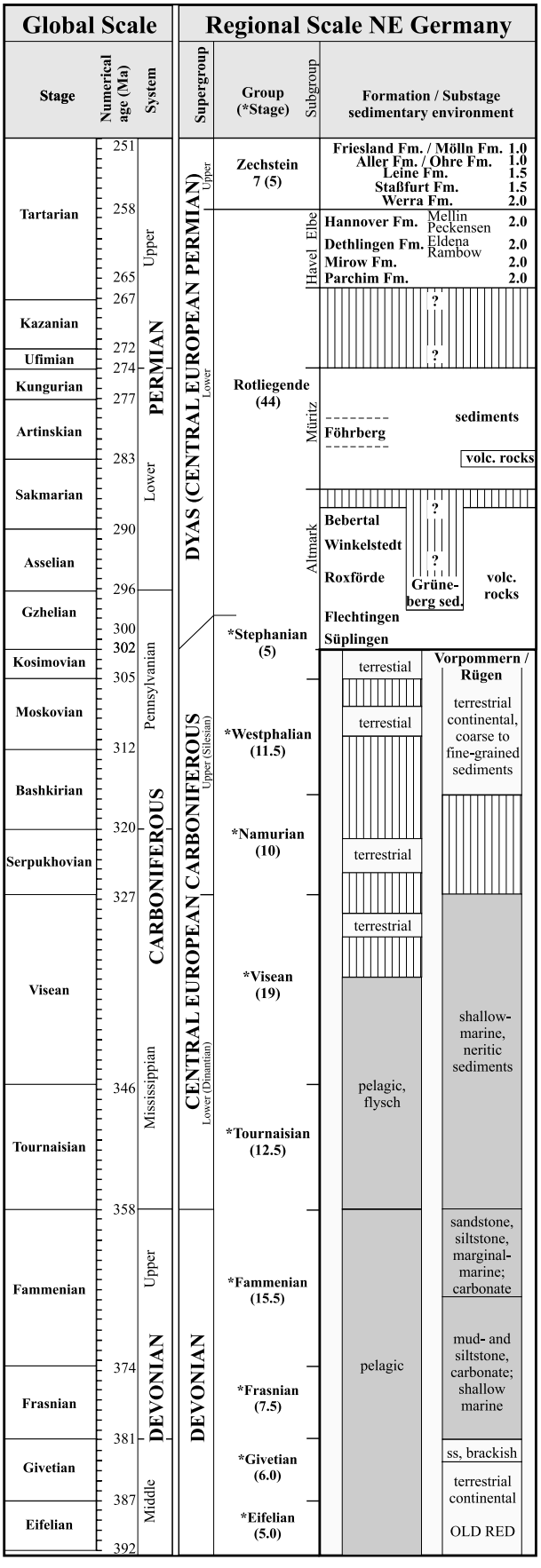

occurrences of the volcanic rocks can be attributed to three larger provinces (Benek et al., 1996) (Figure 1, inset map). First, the Altmark Flechtingen Subhercyn (AFS) region is composed of a large variety of volcanic rocks (mainly rhyolites, some andesites, and some tholeiitic to alkali basalts) and represents one of the greatest eruption centers of the Permian–Carboniferous in the central European basin system. Second, the area of Mecklenburg Vorpommern (MV) and Rügen is composed of rhyolites and subordinately of basalts and andesites. Third, the volcanic association of East Brandenburg (EBB) comprises predominantly basaltic (Mg) andesites.

Persistent thermal uplift in the Permian–Carboniferous resulted in an extensive denudation, and a significant hiatus before thermal subsidence and reactivation of the fault systems formed an area that became increasingly larger and in which, first, the clastic rocks of the lower central European Permian (Rotliegende) (Figure 3) and later by marine transgression the upper central European Permian (Zechstein) mudstones and evaporites were deposited. After the Permian, the NEGB was filled with Mesozoic to Cenozoic (Quaternary) sediments.

FACIES AND DIAGENESIS OF UPPER PALEOZOIC SEDIMENTS

Middle Devonian Eifelian and Givetian sediments were encountered in boreholes of the Vorpommern–Rügen area (Variscan-age foreland basin) (Hoth et al., 1993). Two different sequences (Figure 3) were distinguished. The lower sequence is composed of clayey to silty, poorly sorted sandstones of the terrestrial continental Old Red facies, whereas the upper sequence (Givetian) comprises well-sorted siliceous sandstones and subordinate marlstones (Franke, 1990). Upper Devonian Frasnian and Fammenian sediments consist of shallow-marine to marginal-marine sediments: carbonate, marlstone, marly mudstone, sandstone, and siltstone. Coarse-grained sediments are scarce (Hoth, 1997). In contrast to the marine sediments in the Variscan foreland basin to the north,

Figure 3. Stratigraphy of the upper Paleozoic in the Northeast German Basin (NEGB) (modified from the German Stratigraphic Commission, 2002). For convenience, the Dethlingen and Hannover formations (Plein, 1995) were subdivided according to Katzung et al. (1977).

Devonian rocks in the Variscan fold and thrust zone (Flechtingen area, Figure 3) in the south reflect a pelagic milieu with flysch sedimentation.

The Carboniferous Tournaisian and Visean (Mississippian, cf. Figure 3) are characterized by the clastic terrigenous Culm facies in the south and the Carboniferous Limestone facies in the Variscan foreland basin in the north. The area of transition between the two facies domains is unknown. For the Carboniferous Namurian, Westphalian, and Stephanian (Mississippian and Pennsylvanian, cf. Figure 3), some significant hiatuses are known. Thus, the central and northern Rügen area is devoid of Namurian deposits. Farther south in Vorpommern, Namurian and Westphalian sediments reflect mainly terrestrial mud-flat conditions with local coal deposits. The central part of the NEGB consists of carbonaceous mudstones and siltstones with subordinate coal seams. Westphalian and Stephanian sediments in the northern region represent both alluvial-fan environment and sand-flat environment.

Near the end of the Carboniferous, the humid climate increasingly became arid and was responsible for fluvial and eolian processes forming the Permian Rotliegende sediments (Figure 3). These sediments represent different sedimentary facies (Glennie, 1998). Studies in the NEGB (e.g., Gast et al., 1998) have shown that in the proximity of the basin's margins (the supply areas), braided-plain deposits and alluvial fans are dominant. In distal areas, mud-flat and playa-lake sediments are present. The transition zone between proximal and distal areas of sediment supply is dominated by sediments of fluvial origin; lacustrine and sabkha sediments are subordinate. A few eolian sediments, preserved mainly at the southern margin of the basin, are reworked fluviatile deposits. The Altmark and Müritz subgroups of the Rotliegende (Figure 3) consist of fluvial-lacustrine siltstones and mudstones interbedded with pebbly sandstones and breccias (Gebhardt et al., 1995). Because these sediments are preserved only in local depressions, information about their facies development is scarce. In the lower Havel Subgroup (Parchim Member), braided-plain deposits are prevalent, which change to sand-flat sediments in the basin center. During deposition of the Mirow Member, the silty and muddy sediments of the mud-flat facies became more widespread, and the interbedded fluviatile sandstones retreated. During deposition of the Elbe Subgroup (time of main basin subsidence), fluviatile sandstones are typical particularly in the south, whereas in the north, where the basin was passive, muddy sediments predominate (Plein, 1995). In the basin center, perennial playa-lake, cyclic mud sediments and salt sediments were deposited at that time. The mud-flat facies expanded during Elbe time, so that the fluviatile influence at the margin decreases (Rieke, 2001).

Later, these sediments were compacted and cemented. Early to late diagenetic cements are illite, quartz, albite, anhydrite, calcite, dolomite, haematite, halite, barite, siderite, and chlorite (Schmidt Mumm and Wolfgramm, 2002). Baisert (1990) describes the basin center as an anhydrite- and halite-marked diagenetic province and the basin margin as an area of variable and often incomplete cementation, in which quartz and feldspar dominate. This implies that the effective porosity of the rocks, on average, is lower in the basin center than at the margin. Gast et al. (1998) report a correlation between facies and cementation and show that the sabkha-type sandstones exhibit up to 50% of anhydrite-halite cements, whereas the eolian sandstone at the basin margins contain nearly 100% quartz-feldspar cements.

SAMPLING

For laboratory measurements, mostly the Permian Rotliegende (Figure 3) clastics were sampled from the drill-core archives. Because sedimentary rocks of the Altmark and Müritz subgroups are preserved almost exclusively in local structural lows, most samples were from the younger Havel and Elbe subgroups covering the entire basin. Few samples were obtained from the Devonian and Carboniferous sedimentary succession. Samples of Permian–Carboniferous volcanic rocks are from different magmatic provinces and comprise rhyolites, andesites, and tholeiitic and alkali basalts.

The drill cores sampled were primarily from boreholes (Figure 4) in which good-quality temperature logs are available for heat-flow determination (B. Norden, 2005, unpublished data). Well logs suitable for the study were selected whenever they were available.

BACKGROUND ON THERMAL PROPERTIES

Thermal Conductivity

Thermal conductivity is dependent on composition and geometry of the rock matrix, on porosity, and on pore medium. Additional influences in the situation

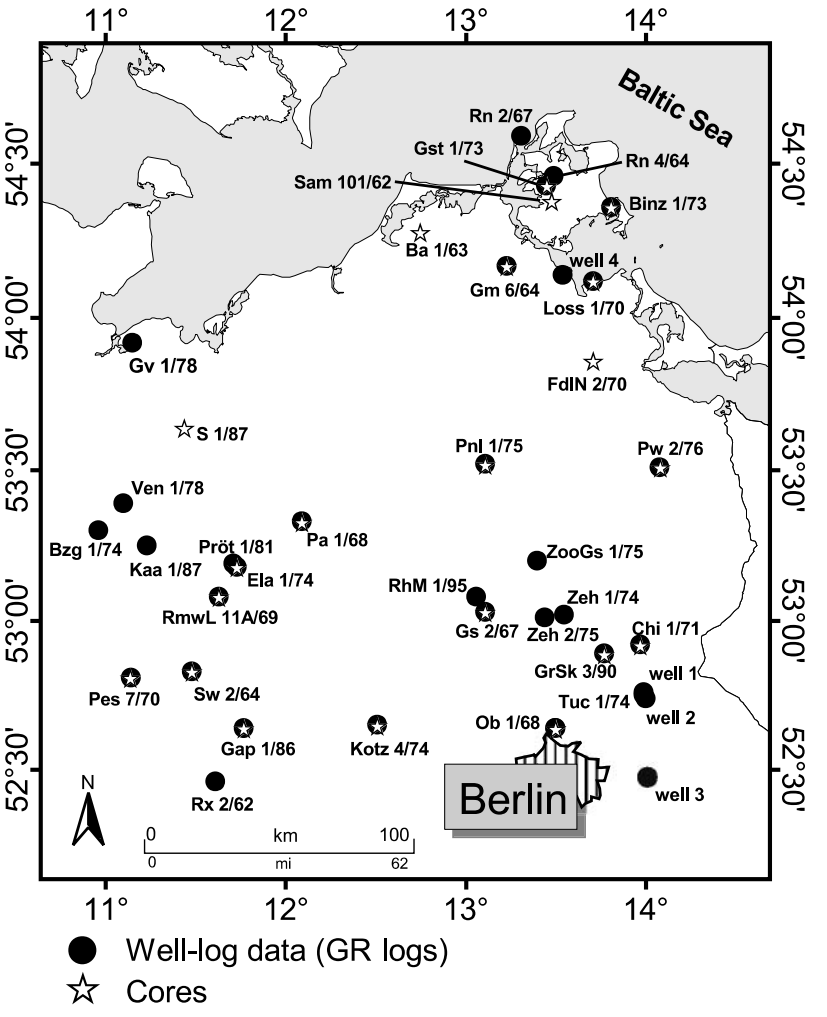

Figure 4. Borehole sites from which cores were collected in the archives of the geological surveys and of the oil and gas industry and from which gamma-ray (GR) logs were used for the determination of radiogenic heat production.

of a deeply buried rock are pressure and temperature (e.g., Schön, 1996). Measurements of thermal conductivity cover a wide spectrum of techniques that can be subdivided into direct (laboratory) and indirect (well-logging) approaches. In the past, the most used direct method has been the steady-state divided-bar technique, where either saturated or nonsaturated rock was investigated. Other techniques use transient heat sources. For example, line sources are deployed in the pulsed line-source approach (Lewis et al., 1993) and in the needle-probe technique and the half-space line-source methods. The latter two techniques are described and referenced in more detail by Blackwell and Steele (1989) and Pribnow and Sass (1995). A different type of direct method recently introduced is termed ''optical scanning'' (Popov et al., 1999). This method is based on scanning a sample surface with a focused, movable heat source in combination with a temperature sensor. Comparison of results from divided-bar, line-source, and optical-scanning measurements (Popov et al., 1999) has shown that all these methods work equally well within their combined error, producing consistent results. However, the optical-scanning method excels in its high precision (1.5%) and accuracy (1.5%) and a short time of measurement, as well as a recording of the thermal-conductivity distribution along a scanning line on a sample. The thermal-conductivity distribution enables a detailed study of the heterogeneity of the sample. Therefore, the technique is also of special interest for studying the physical properties of porous sedimentary rocks under dry and fluid-saturated conditions (Popov et al., 2003; Hartmann et al., 2005).

Recently, studies focused on determining thermal conductivity from well logs. Although this approach could circumnavigate the problem of biased single-point rock sampling for laboratory measurements and could provide thermal-conductivity values along the entire borehole profile, its use was precluded in the NEGB because of poor quality and the limited number of logs available.

Radiogenic Heat Production

Rocks exhibit a natural radioactivity caused by the decay of natural radionuclides (e.g., Schön, 1996). The three types of isotope decay series abundant in rocks are the uranium series (decay of ^{238}U and ^{235}U), the thorium series (decay of ^{232}Th), and the decay of the potassium isotope ^{40}K. The radioactive heat generation (A) in $\mu W/m^3$ as a result of isotope decay is expressed after Rybach (1976) as

$$A = \rho\ (9.52\ U + 2.56\ Th + 3.48\ K)\ 10^{-5} \quad (1)$$

where ρ is density of the rock (in kg/m^3), U and Th are the contents of uranium and thorium (in ppm), and K is the content of potassium (in wt.%).

The whole rock abundances of U, Th, and K, in principle, can be determined by chemical analysis, by gamma-spectroscopic measurements, and from gamma-ray (GR) borehole logs. The latter approach developed by Bücker and Rybach (1996) uses a linear relationship between natural total gamma-ray logs from industrial exploration (in API units; see Anonymous, 1974) and laboratory-measured heat production (A, $\mu W/m^3$):

$$A = 0.0158\ (GR[API] - 0.8) \quad (2)$$

The equation is validated for API values less than 350° and is estimated to give an error of less than 10%.

THE ANALYSIS

Thermal Conductivity

Thermal conductivity (λ) was determined under dry conditions on 329 core samples (196 samples of Permian [Rotliegende] sedimentary rocks, 53 samples of pre-Permian sedimentary rocks, and 80 samples of Permian–Carboniferous igneous rocks). The measurements were made with an optical-scanning device (Lippmann and Rauen, GbR) using the principle and the sample preparation as described by Popov et al. (1999). Sample thickness was greater than 3 cm (1.2 in.), and the length of the core samples was greater than 4 cm (1.6 in.). The error of determination was less than 3%.

Measurements were performed (1) in the direction of principal (vertical) heat flow (on the top or bottom of a cylindrical drill-core sample) and (2) perpendicular to this direction (on a plane along the vertical core axis). For most of the Lower Permian sediments, these directions of measurement give principally the thermal conductivity perpendicular to bedding ($\lambda_\perp$) in situation 1, and a thermal conductivity parallel to bedding ($\lambda_{||}$) in situation 2. The ratio of the measured maximum thermal conductivity (λ_{max}) to the measured minimum thermal conductivity (λ_{min}) is the anisotropy ratio (An).

Thermal conductivity determined on dry samples was corrected to saturated conditions using the geometric mean model (see, e.g., Woodside and Messmer, 1961a, b):

$$\lambda_{geo} = \lambda_{matrix}^{1-\phi}\ \lambda_{pore}^{\phi} \quad (3)$$

where λ_{geo} is thermal conductivity according to the geometric mean; λ_{matrix} is thermal conductivity of the matrix; λ_{pore} is thermal conductivity of the pore fill (air = 0.026 W/m/K or water = 0.6 W/m/K); and ϕ is the porosity. On a subsuite of samples, thermal conductivity was measured under water-saturated conditions (λ_{satm}), which allowed a comparison with a calculated thermal conductivity for water saturation (λ_{satc}). Porosity needed in these calculations was determined by the mass change between dehydrated and saturated states of the sample (Archimedes' method). Samples first were dried at 60°C and then saturated by submerging them in water inside a sealed vacuum chamber. Modal analyses (Rieke, 2001; this study) were used to describe the pore cements.

Radiogenic Heat Production

The contents of U, Th, and K were measured by chemical analysis in 34 samples. Uranium and thorium was determined by inductively coupled-plasma mass spectrometry (ICP-MS; Perkin-Elmer/Sciex Elan Model 5000a) according to the method and with the precision and accuracy outlined by Dulski (2001). Potassium was analyzed by wavelength-dispersion x-ray fluorescence spectrometry (XRF; Bruker/Model axs SRS303-AS, SPECTRA 3000 software) using fused lithium tetraborate discs. The contents of U, Th, and K of Permian–Carboniferous magmatic rocks were complemented by other data (R. Benek, 1995, personal communication; Benek et al., 1996).

In addition, in 18 samples, the concentrations of U, Th, and K were determined by gamma-ray spectrometry using a coaxial germanium semiconductor detector (HPGe, p type; EG&G Ortec/Perkin Elmer Instruments). The detector, based on the gaseous electron multiplier technology, has a resolution of 1.71 keV

(1.33 MeV, ^{60}Co, 6 μs), a peak-to-Compton ratio (which is the key indicator of a detector's ability to distinguish low-energy peaks in the presence of high-energy sources) of 70 (^{60}Co, 6 μs), and a relative efficiency of 41.1% (1.33 MeV, ^{60}Co, 6 μs). It was placed in cylindrical, 10-cm (4-in.)-thick old lead shielding to reduce background radiation originating from building materials and cosmic rays. This compartment was lined with 2-mm-thick copper to absorb secondary radiation. An amount of about 400 g of each sample was placed in a Marinelli beaker after the sample was crushed to less than 2 mm and rested for 2–3 weeks to adjust to radioactive steady state. The relative error for the determination of the U content is 11%, and the relative error for the determination of the Th and K content is 5 and 1%, respectively.

Total-count gamma-ray (GR) logs were available for this study. These logs, routinely obtained in the NEGB until the 1990s during hydrocarbon exploration, were measured with Geiger–Müller counters calibrated using Co-60 emitters (S. Fricke, 2001, personal communication) and recorded in GEs (Gamma-Einheiten). The logs were corrected first for the borehole conditions (borehole diameter and density of the drilling mud) and second, for the size and position of the recording unit used. Logs of a generally abnormal character were discarded. Abnormal logs could be either a result of abnormal drill-mud composition (bentonite or KCl mud) or because of gas entry into the well.

To use Bücker and Rybach's (1996) equation (equation 2), an empirical conversion equation was developed based on relating 22 depth intervals of GE logs to API-reading GR logs (Figure 5; Table A1, available as Datashare 21 at www.aapg.org/datashare). The GR logs cover the range of 10–156° API comprising formations of Triassic to Tertiary age. Only normalized GE-log responses in close proximity to wells with GR logs were used to ensure that the wells reflect the same geology. Furthermore, care was taken that only logs were related from wells with similar drill-mud composition. The conversion equation is

$$\mathrm{GR[API_C]} = 4.95\ \mathrm{GR[GE_C]} - 27.24 \qquad (4)$$

where GR[API$_c$] is the predicted gamma-ray value in API and GR[GE$_c$] is the borehole-corrected GE value. The correlation coefficient R for the linear regression is 0.94 (n = 22), and the standard deviation is ±17° API, which implies a reliability of approximately 10% for the predicted API value. Based on equations 2 and 4, the radiogenic heat production (A) was determined by

$$A(\mu\mathrm{W/m^3}) = 0.0783\ (\mathrm{GR[GE_C]} - 5.66) \qquad (5)$$

The total error resulting from equation 5 is predicted to be no larger than 20%.

Finally, rock density was measured on one subset of samples, together with porosity (Archimedes' method), and for another subset of samples using the helium gas pycnometer AccuPyc 1330 (Micrometrics).

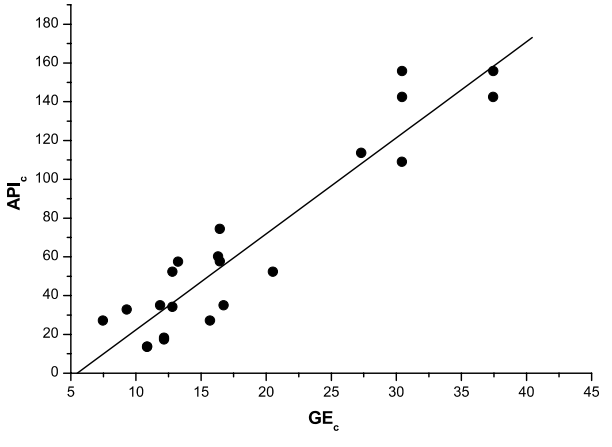

Figure 5. Correlation of gamma-ray GE units and API units for 22 stratigraphic units. Coefficient R of the linear regression is 0.94; standard deviation is ±17° API.

RESULTS

Thermal Conductivity of Lithotypes

Thermal conductivity differs considerably between and within lithotypes (Tables 1, 2; Table A2, available as Datashare 21 at www.aapg.org/datashare). With regard to Permian–Carboniferous magmatic rocks (Table 1), the mean thermal conductivity is highest in the granitoids (3.1 W/m/K) followed by the rhyolites (2.9 W/m/K). The lowest values are observed in basalt (2.2 W/m/K) and in dolerite (2.0 W/m/K). The decrease in thermal conductivity is related to a decrease in the SiO_2 content, which is, in rhyolite, 72.1 ± 1.7 wt.% (n = 15); in trachyte and dacite, about 65.2 ± 1.8 wt.% (two samples each); in andesite, 55 ±2.6 wt.% (n = 10); and in basalt, 46.8 ±1.1 wt.% (n = 4). For the dolerite (from the island of Rügen; borehole Gst 1/73, Figure 4) a SiO_2 content of about 43.2 wt.% was reported by R. Benek (1995, personal communication). The volcanic rocks and granitoids show practically no anisotropy.

Table 1. Thermal Conductivity ($\lambda_\perp$, in W/m/K) of Saturated Permian–Carboniferous Magmatic Rocks*

Rhyolite				Trachyte				Dacite				Andesite				Basalt				Dolerite				Granitoids			
λ	Range	Mean	*n*	λ	Range	Mean	*n*	λ	Range	Mean	*n*	λ	Range	Mean	*n*	λ	Range	Mean	*n*	λ	Range	Mean	*n*	λ	Range	Mean	*n*
2.2	3.4	2.9	25	2.1	3.0	2.5	2	2.1	2.4	2.3	4	1.9	2.9	2.3	21	1.9	2.7	2.2	6	1.7	2.3	2.0	5	2.9	3.5	3.1	8

*Only measurements in the direction of the principal (vertical) heat flow are shown. For details of data and λ determined perpendicular to the vertical depth ($\lambda_{||}$), see Table A2.

In clastic rocks and carbonates, thermal conductivity measured perpendicular to bedding ($\lambda_\perp$; Table 2) is lowest in mudstone and siltstone (2.3–3.6 W/m/K). Values for conglomerates (3.2–3.4 W/m/K) are at the upper bound of the mudstone-siltstone range. The largest variability is observed in the sandstones (2.6–4.8 W/m/K), which also exhibit the highest values measured. A few carbonate samples show a mean value of 2.5 W/m/K. In general, except for the carbonates, the thermal conductivity of each sedimentary lithotype depends strongly on mineralogy (cementation) and porosity (see text below).

As expected, thermal conductivity measured parallel to bedding ($\lambda_{||}$; Table A2) shows higher values (e.g., Schön, 1996). However, the mean anisotropy of thermal conductivity is small (1.05–1.21). Mudstone (1.21) and siltstone (1.16) have the highest ratios as a result of phyllosilicates oriented along bedding during compaction. Carbonates show a mean anisotropy of 1.10; sandstones show a mean anisotropy of 1.09; and conglomerates show a mean anisotropy of 1.05. The anisotropy in the sandstones and conglomerates is affected by the habitat and texture of grains and pores instead of the orientation of phyllosilicates, which are less dominant in these rocks. The results on anisotropy of thermal conductivity confirm that the rocks investigated can be classified as less stratified, so that an isotropic rock model (e.g., the geometric model) for correcting dry-measured thermal conductivity into saturated values seems justified.

Most sedimentary rock samples in this study were encountered from depths of 3000–5000 m (9800–16,400 ft). These rocks are compacted and consolidated so that expected changes in porosity resulting from different burial depth should be small. Although a weak trend of porosity decrease with increasing depth is observed for Rotliegende sediments (Figure 6A), no such trend is observed when plotting thermal conductivity with depth (Figure 6B). Therefore, most of the variability in thermal conductivity has to be attributed to changes in mineral composition (grains and cements). In fact, the quartz content of the rocks does mainly control the thermal conductivity (Table 3). Rocks in which clay cements prevail show distinctively lower values than rocks with silica (quartz) cements. In addition to these two major groups of cements, variable content of anhydrite, calcite, and Fe minerals (hematite) also affects the overall variation of thermal conductivity shown in Figure 6B. For example, two sandstone samples of the Elbe Subgroup (Ob-N07 and Ob-N08, Table A2) from the Ob 1/68 borehole exhibit similar

Table 2. Thermal Conductivity ($\lambda_{\perp}$, in W/m/K) of Saturated Clastic Rocks and Carbonates Measured Perpendicular to Bedding*

Stratigraphic Description	Mudstone				Siltstone				Sandstone				Conglomerate				Limestone-Marlstone			
	λ	Range	Mean	*n*	λ	Range	Mean	*n*	λ	Range	Mean	*n*	λ	Range	Mean	*n*	λ	Range	Mean	*n*
Elbe Subgroup	1.5	3.8	2.3	18	1.7	5.5	2.9	25	1.9	5.3	4.0	56	2.4	3.4	3.2	6				
Havel Subgroup	1.9	4.2	2.8	6	2.3	3.9	2.9	13	2.3	5.3	4.2	30	2.7	4.2	3.3	6				
Müritz Subgroup									2.5	2.7	2.6	2	2.4	3.9	3.2	9				
Altmark Subgroup							2.3	1					2.6	4.3	3.4	2				
Stephanian									4.3	5.5	4.7	5								
Westphalian	2.9	4.6	3.6	3	2.6	4.1	3.4	11	2.7	6.0	4.6	18								
Namurian							3.0	1	3.3	4.0	3.6	4								
Visean			2.7	1													2.2	2.7	2.5	2
Frasnian																	2.0	3.0	2.5	3
Givetian									2.1	6.0	4.8	3								
Eifelian							3.6	1												

*For details of data and λ determined parallel to bedding ($\lambda_{||}$), see Table A2.

porosity (7.4 and 6.7%, respectively) but have different measured $\lambda_{\perp sat}$ values of 3.8 and 5.0 W/m/K, respectively. Modal analyses of these samples depict that the thermal conductivity correlates with the quartz grain content and the quartz cement content (Ob-N08: 66.7% quartz grains and 16.7% quartz cement; Ob-N07: 59.1% quartz grains and 1.0% quartz cement). In addition, Ob-N07 is characterized by a higher content of other matrix minerals (such as illite, 12.4%), whereas Ob-N08 is almost devoid of other matrix minerals (0.9%). Because of the lower average thermal conductivity of phyllosilicates compared to quartz (e.g., Brigaud and Vasseur, 1989), the difference in thermal conductivity between these two sandstone samples obviously is a result of their different mineral assemblage.

Although the samples in this study are of low average porosity (<3%), porosity and type of pore fill do influence the bulk thermal conductivity. To investigate this relation, the ratios between thermal conductivity of measured water-filled samples and thermal conductivity of air-filled samples were crossplotted versus porosity (Figure 7). Because of the higher thermal conductivity of water than of air, the ratios are greater than 1. The following features are striking: (1) the measured ratios are positively correlated; (2) the ratios generally are higher as the corresponding theoretical values provided by the geometric-mean model. The deviations from the theoretical values are larger for the ratios of $\lambda_{\perp}$ than for those of $\lambda_{||}$ (not shown graphically). This observation is most likely a result of the internal structure (microfractures oriented parallel to bedding) of the rock sample (see Popov et al., 2003).

The average misfit between measured water-saturated and calculated water-saturated thermal conductivity amounts to ±0.35 W/m/K. The discrepancy in most of the observations is less than ±10% (Figure 8A) and seemingly affected by lithotype instead of by porosity (Figure 8B). For example, the largest difference between calculated and measured water-saturated thermal conductivity is in low-porosity sandstone samples (ϕ < 5%). In samples with higher porosities, the difference is less, and the calculated values are both overestimates and underestimates. In the calculation of formation thermal conductivity, the measured values, if available, were preferred.

Thermal Conductivity of Geologic Formations

First, the proportion of different rock types in the formation was obtained using the descriptions from sample logs and gamma-ray logs and other available well-logging data. Formation thermal conductivity (Tables 4, 5) was then determined based on the thermal conductivity of lithotypes (mudstone, siltstone, sandstone, conglomerate, limestone-marlstone, Table 2) making up the formation. For the salt lithotype, a value of 4.8 W/m/K was used. For the two formations with the most data (the Elbe and Havel subgroups, Table 4), thermal conductivity was determined in two ways. In case I, the cementation of the rock type was considered using the data in Table A2; in case II, the bulk lithotypes were considered. However, the difference between the case I and case II values is small and on the order of ±0.2 W/m/K,

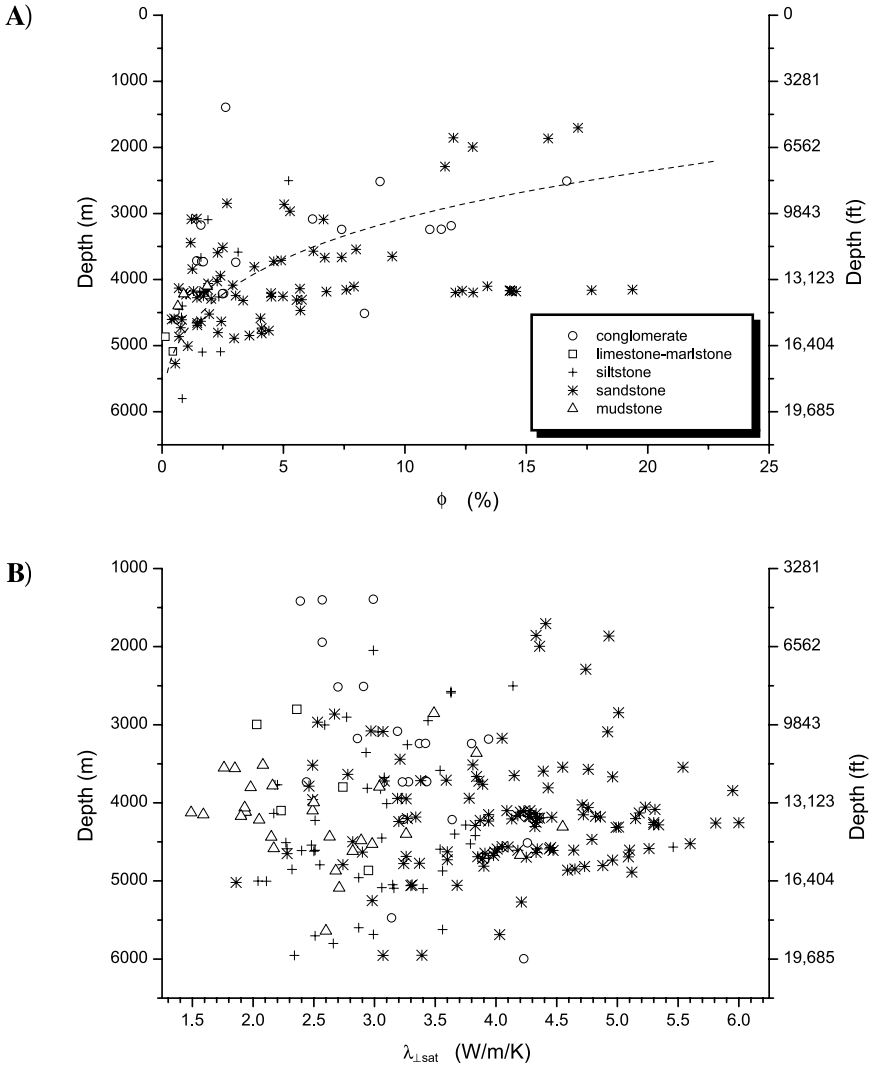

Figure 6. (A) Influence of burial depth on porosity (ϕ) of sedimentary rocks and (B) saturated thermal conductivity measured perpendicular to bedding ($\lambda_{\perp sat}$) versus depth. $\lambda_{\perp sat}$ was plotted instead of $\lambda_{||}$ values because it reflects the effective thermal conductivity for heat-flow determination.

not exceeding 0.5 W/m/K. Consequently, the mean formation thermal conductivity of the two subgroups also does not differ significantly in the two scenarios (Elbe Subgroup; 3.2 W/m/K [case I] and 3.3 W/m/K [case II]; Havel Subgroup: 3.7 W/m/K [case I] and 3.9 W/m/K [case II]). The higher values of the Havel Subgroup are caused by the basinwide occurrence of sand-flat deposits (mostly coarse-grained rocks showing predominantly quartz cementation).

At a basinwide scale, the formation thermal conductivity of both subgroups varies remarkably. For example, the regional variation of values in the Elbe

Table 3. Thermal Conductivity (λ) of Sedimentary Rock Dependent on Type of Cementation*

	Quartz Cement			Clay-Matrix Cement			Deviation
Lithology	λ (W/m/K)	Standard Deviation	*n*	λ (W/m/K)	Standard Deviation	*n*	λ (W/m/K)
Sandstone	4.6	0.7	54	3.2	0.5	15	1.4
Siltstone	3.5	0.5	13	3.0	0.5	9	0.5
Mudstone	3.4	0.7	4	2.4	0.3	10	1.1

*Values are based on data in Table A2 and represent the mean of $\lambda_{\perp}$ and $\lambda_{||}$ values.

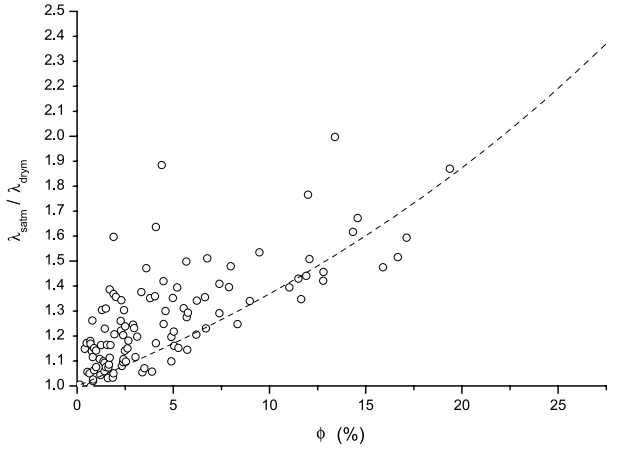

Figure 7. Influence of different pore medium on bulk thermal conductivity for $\lambda_{\perp}$. The ratio of measured water-saturated (λ_{satm}) over measured air-saturated thermal conductivity (λ_{drym}) is plotted as a function of porosity (ϕ). For comparison, the dashed line represents the trend of values calculated on the basis of matrix thermal conductivity and porosity using the geometric-mean model (equation 3).

Subgroup amounts to 0.8 W/m/K (case I) and 0.4 W/m/K (case II), and the respective values in the Havel Subgroup amount to 1.1 and 0.8 W/m/K. Neither the case I nor case II values are, in general, higher. Although for the NEGB, the formation thermal conductivity was expected to be higher in the basin center (because of higher percentage of salt intercalations) than at the basin margin, no such correlation was observed. The higher thermal conductivity of salt compared to most of the clastic rocks is offset by the lower thermal conductivity of clastic rock in which the salt is embedded. At the basin margin, coarse-grained sediments (in places with extensive quartz cementation) are the reason that formation thermal conductivity is higher. This also explains the high formation value of 3.7 W/m/K in the GrSk 3/90 borehole, where the Elbe Subgroup was deposited under fluvial conditions, and the lower Elbe Subgroup (Rambow Member) contains eolian sediments (reworked fluviatile deposits with a high content of quartz).

For the Müritz and Altmark subgroups, formation thermal conductivity was not calculated because of the few samples available (Table 2). However, because these subgroups are preserved only locally, the lack of data is insignificant for an evaluation of overall thermal conductivity of the Permian Rotliegende. Thermal conductivity of the Devonian and Carboniferous formations (Table 5) is considered to be only a first approximation, also because of only few data available. Nevertheless, the range of 2.6–4.2 W/m/K observed is reasonable for most of the units of pre-Permian age. The Frasnian (Upper Devonian), comprising marlstone (45%), mudstone (36%), and siltstone (14%), shows a formation thermal conductivity of 2.6 W/m/K, and the Givetian (Middle Devonian), because of a higher content of quartzitic sandstones, shows a value of 4.2 W/m/K, respectively.

Radiogenic Heat Production of Permian–Carboniferous Magmatic Rocks

In general, heat production (Table 6) increases from mafic rock (basalt) toward silicic rock (granite, rhyolite). Within a particular rock type, heat production can vary considerably. The tholeiitic basalts of Rügen and the AFS area (Figure 1) show a heat production

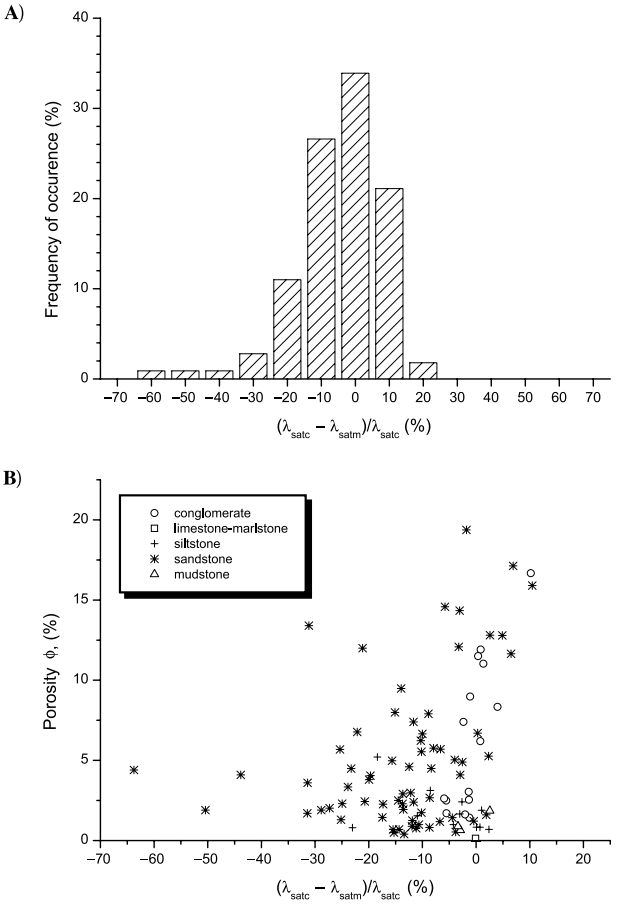

Figure 8. Comparison between measured water-saturated (λ_{satm}) and calculated water-saturated thermal conductivity (λ_{satc}) for $\lambda_{\perp}$. (A) Histogram of the deviations (n = 109). (B) Porosity (ϕ) versus deviations.

Table 4. Formation Thermal Conductivity (TC) of Rotliegende Sediments Derived at Different Borehole Locations*

A) Elbe Subgroup

	Case I														Case II								TC (W/m/K)		Total Thickness (m)
	%							λ (W/m/K)							%				λ (W/m/K)						
	ms		si		ss			ms		si		ss													
Borehole	Type 1	Type 2	Type 1	Type 2	Type 1	Type 2	salt	Type 1	Type 2	Type 1	Type 2	Type 1	Type 2	salt	ms	si	ss	salt	ms	si	ss	salt	Case I	Case II	
Pw 1/74	52		10		38			1.9		2.5		4.6			52	10	38		2.5	3.1	4.0		3.0	3.1	171
Sw 2/64	23		21		56			2.0		3.1		4.2			23	21	56		2.5	3.1	4.0		3.5	3.5	402
Gap 1/86	20		23		35	22		2.5		3.1		4.4	3.8		20	23	57		2.5	3.1	4.0		3.6	3.5	354
GrSk 3/90		4		48		47			2.3		3.1		4.4		4	48	47		2.5	3.1	4.0		3.7	3.5	349
Pa 1/68	1	23	21	43	5	7	1	2.5	2.8	2.8	2.9	3.3	4.4	4.8	24	64	12	1	2.5	3.1	4.0	4.8	3.0	3.1	815
RmwL 11A/69	27		32		21	15	5	2.4		2.9		3.3	3.8	4.8	27	32	36	5	2.5	3.1	4.0	4.8	3.1	3.3	694
Gs 2/64		15		46	25	14			2.3		3.1	3.4	4.4		15	46	38		2.5	3.1	4.0		3.2	3.4	443
Ela 1/74	14	14	19	26	9	15	3	2.5	3.0	2.8	2.8	2.4	3.3	4.8	28	46	23	3	2.5	3.1	4.0		2.9	3.2	677
Barth 1/63	18		66		16			2.5		3.0		3.1			18	66	16		2.5	3.1	4.0		2.9	3.1	221
Mean																							3.2 ± 0.3	3.3 ± 0.2	

B) Havel Subgroup

	Case I														Case II								TC (W/m/K)		Total Thickness (m)
	%							λ (W/m/K)							%				λ (W/m/K)						
	ms		si		ss			ms		si		ss													
Borehole	Type 1	Type 2	Type 1	Type 2	Type 1	Type 2	cg	Type 1	Type 2	Type 1	Type 2	Type 1	Type 2	cg	ms	si	ss	cg	ms	si	ss	cg	Case I	Case II	
Pa 1/68		6		44		48	3		2.5		3.2		4.2	4.0	6	44	48	3	3.0	3.2	4.3	3.3	3.6	3.7	494
RmwL 11A/69		42		2		56			2.3		3.2		3.8		42	2	56		3.0	3.2	4.3		3.2	3.7	269
Gap 1/86		0		0		100							4.3		0	0	100				4.3		4.3	4.3	219
Gs 2/64		2		24		74			2.3		3.2		4.7		2	24	74	3	3.0	3.2	4.3		4.2	4.0	139
Ela 1/74	18		47		35			3.1		3.2		3.8			18	47	35		3.0	3.2	4.3		3.4	3.5	267
Mean																							3.7 ± 0.5	3.9 ± 0.3	

*The percentage (%) of lithotypes making up the formation and the thermal conductivity (λ) of each lithotype are given. In case I, lithotypes are subdivided into subtypes according to different cementation. In part A of the table, type 1 refers to clay-matrix cement, and type 2 refers to halite-, quartz-, or anhydrite-dominated cement. In part B of the table, type 1 refers to calcite cement (anhydrite and quartz cements are subordinate), and type 2 refers to anhydrite or quartz cement. In case II, bulk lithotypes are considered. The λ of the lithotypes reflects mean values from $\lambda_{\perp}$ and $\lambda_{||}$ according to Table A2. The total thickness of the formations is given. Abbreviations: cg = conglomerate; ms = mudstone; si = siltstone; ss = sandstone.

Table 5. Formation Thermal Conductivity (TC) of Pre-Permian Units Derived at Different Borehole Locations*

A) Stephanian

Borehole	% ms	% si	% ss	% cg	λ ms	λ si	λ ss	λ cg	TC (W/m/K)	Total Thickness (m)
Barth 1/63	16	47	37		3.0	3.2	4.9		3.8	210
Binz 1/73	38	15	47		2.8	3.2	4.7		3.7	388
Mean									3.8	

B) Westphalian

Borehole	% ms	% si	% ss	%	λ ms	λ si	λ ss	λ	TC (W/m/K)	Total Thickness (m)
Ela 1/74	18	36	46		3.0	3.2	3.5		3.3	355
Barth 1/63	25	52	22	1**	3.2	3.6	4.7	0.3**	3.7	1085
Binz 1/73	35	19	38	8†	3.2	3.6	4.7	2.1†	3.9	836
Mean									3.7	

C) Namurian

Borehole	% ms	% si	% ss	%	λ ms	λ si	λ ss	λ	TC (W/m/K)	Total Thickness (m)
Gs 2/64	13	27	60		3.0	3.2	4.2		3.8	192
Ela 1/74		88	12			3.2	4.2		3.4	76
Barth 1/63	41	45	12	2**	3.0	3.2	3.8	0.3**	3.1	166
Mean									3.5	

D) Frasnian–Eifelian (Binz 1/73 borehole)

	% ms	% si	% ss	% mm	%	λ ms	λ si	λ ss	λ mm	λ	TC (W/m/K)	Total thickness (m)
Frasnian	36	14		45	4†	2.7	2.7		2.5	2.1†	2.6	371
Givetian	8	37	53		2†	3.2	3.6	4.8		2.1†	4.2	648
Givetian–Eifelian	9	42	48		2†	3.2	3.6	4.8		2.1†	4.1	439
Eifelian	18	44	37		2†	3.2	3.6	4.8		2.1†	3.9	777

*The percentage (%) of lithotypes making up the formation and the thermal conductivity (λ) of each lithotype calculated on the basis of the mean values from $\lambda_{\perp}$ and $\lambda_{||}$ (Table A2) are given. The total thickness of the formation is noted. cg = conglomerate; mm = marlstone; ms = mudstone; si = siltstone; ss = sandstone.
**Adopted thermal-conductivity value for coal (after Čermak et al., 1982).
†Adopted thermal-conductivity value for dolerite (after Čermak et al., 1982).

of less than or equal to 0.3 μW/m^3, whereas the alkaline and transitional basalts (restricted to the AFS area) have slightly higher values (0.7–0.9 μW/m, Table 6). Basaltoids of Rügen show a mean value of 0.4 μW/m^3 in well logs (Table 7), implying that these rocks may belong to the group of transitional-type basalts. Andesitic rocks exhibit a range of 0.4–2.8 μW/m^3 (Table 7), with the mantle-derived Mg-andesites of the EBB region (Table 6) being at the lower end of this range (0.7 μW/m^3 on average). Rhyolites display a heat production in the range of 2.1–5.9 μW/m^3, with the highest values observed in the AFS province (Table 7). Values for the rhyolites in the EBB and in MV range between 2.2–2.9 and 2.4–4.1 μW/m^3, respectively. The few granites

encountered by boreholes in the northern and southwestern part of the basin have a heat production between 2.7 and 4.0 μW/m^3.

Radiogenic Heat Production of Sedimentary Rocks

Application of the conversion equation (equation 5) shows heat-production values similar to those obtained by laboratory measurements (for an example, see Figure 9). Discrepancies between well-log-derived and laboratory values observed at some borehole locations (Table 8; Tables A3, A4, available as Datashare 21 at www.aapg.org/datashare) are nonsystematic and assumed to be influenced by the sampling interval only. Values of the Permian Rotliegende and the Carboniferous Westphalian (Pennsylvanian) rocks range between 0.4 and 3.1 μW/m^3 (Tables A3, A4). In detail, the sandstones (composed mostly of quartz and subordinate feldspar and rock fragments) exhibit lower values (range 0.4–2.2 μW/m^3, mean 1.0 μW/m^3, Table 8) than siltstones-mudstones (range 1.3–3.1 μW/m^3, mean values 1.8–2.5 μW/m^3, Table 8) of higher mud and clay content and, consequently, higher potassium content. This is a well-known tendency described in detail by Schön (1996). The mudstone values are close to the level of values determined for Permian–Carboniferous rhyolitic and andesitic rocks (Table 7). Considering that the fine-grained Rotliegende clastic rocks originate from these volcanic rocks (Rieke, 2001), it is assumed that the relatively high heat production in these sediments is not a local phenomenon but typical for larger regions in the basin.

Heat production of geological formations, from Devonian to Quaternary, is shown in Table 9 and in more detail in Table A5, available as Datashare 21 at www.aapg.org/datashare. The Cenozoic formations (Paleogene, Neogene, and Pleistocene) made up of silt, sand, and clay show a heat production in the range of 0.9–1.3 μW/m^3. Values for the Mesozoic formations (Triassic, Jurassic, and Cretaceous) are similar (0.6–1.8 μW/m^3), whereas the lower values relate to carbonate sequences composed of limestone, dolomite, marl, and chalk (e.g., the Upper Cretaceous and the Triassic Muschelkalk), and the higher values refer to clastic sequences made up of sandstone, siltstone, mudstone, and shale (e.g., the Triassic Buntsandstein and Keuper formations). The Permian Zechstein (mostly salt, anhydrite, and limestone) shows the lowest mean heat production (0.4 μW/m^3).

Mean heat production of the Permian Rotliegende subgroups is on the order of 1.4–2.1 μW/m^3 (range of values 0.9–2.5 μW/m^3, Table 9). An example for values at the lower end of range is the value of the Havel Subgroup in the Kotz 4/74 borehole (Table A4), where the formation consists mainly of sandstone, silty sandstone, and siltstone. The value of the Müritz Subgroup (2.1 μW/m^3) determined in the Gst 1/73 and Pa 1/68 boreholes (Table A4) is at the upper end of range and reflects a large part of conglomerates of rhyolitic fragments and mudstones.

The pre-Permian sediments, which reflect a more diverse sedimentary environment than the Rotliegende, consequently also show a larger variation in mean formation heat production (0.9–2.0 μW/m^3; Table 9; Table A5). The lowest values (0.9–1.2 μW/m^3) are observed in the Devonian (Givetian, Frasnian, and Famennian) and in the Carboniferous Tournaisian (Mississippian) of the Rügen area, where the rocks consist primarily of limestone and marly limestone (mudstone and marly mudstone are scarce; Hoth, 1997).

Because of only one value (2.1 μW/m^3; Ob 1/68 borehole, Table A5) reported for the Carboniferous clastic terrigenous Culm facies in the south, whether the rocks of this facies really differ in heat production from the marine Carboniferous Limestone facies in the pre-Permian foreland basin in the north (mean = 1.4 μW/m^3), where the variability of values is dependent on the content of clay and organic matter in these sediments, cannot be substantiated. In addition, the Culm-facies value was determined in the upper (clayey) 100 m (330 ft) of the formation and, therefore, may overestimate the value for the entire formation.

Mean heat production in the Carboniferous Namurian, Westphalian, and Stephanian (Mississippian and Pennsylvanian) ranges between 1.7 and 2.0 μW/m^3; Table 9). Again, there is only a weak indication that the area to the south has the higher values. Although the Westphalian sometimes is interbedded with coal layers (for example, in the Binz 1/73 borehole [Rügen area] where a 1.5-m [5-ft]-thick hard coal exhibits a heat production of 3.3 μW/m^3, Table A5), the formation value (1.8 μW/m^3) turns out to be moderate. Lower values (1.4 μW/m^3) are encountered in the Gst 1/73 and Rn 4/64 boreholes (also Rügen area), where the Westphalian sediments comprise a larger part of sandstones of less organic content. Another example for the dependence of radiogenic heat production on organic content is in the Bzg 1/74 borehole, where the Namurian sandstone-dominated sequence has a heat production of 1.5 μW/m^3, whereas the younger, Westphalian

Table 6. Contents of K, U, and Th, Rock Density, and Radiogenic Heat Production (*A*)*

Rock Type	Province**	Sample	Type	Depth (m)	K (%)	$N^{\dagger}$	U (ppm)	$N^{\dagger}$	Th (ppm)	$N^{\dagger}$	Density (10^3kg/m^3)	A (μW/m^3)
Basaltic	AFS	Average††	Tholeiitic		0.84	6	0.44	1	1.39	1	2.75	0.3 ± 0.1
rock	AFS	Average††	Transitional		1.12	11	1.60	2	2.70	3	2.75	0.7 ± 0.1
	AFS	Gp-03	Alkaline	4458.3	1.68	1	1.52	1	3.64	1	2.77	0.8
	AFS	Gp-04	Alkaline	4410.0	3.20	1	1.05	1	5.28	1	2.74	0.9
	Rügen	Average††	Tholeiitic		0.41	12	0.07	8	0.33	12	2.80	0.1 ± 0.1
	Rügen	Gst-01	Tholeiitic	1689.3	0.13	1	0.06	1	0.29	1	2.81	<0.1
Andesitic	AFS	Average††	Andesitoide 7‡		3.45	22	5.50	4	16.00	5	2.65	2.8 ± 0.8
rock	AFS	Average††	Andesitoide 8‡		3.35	41	3.10	11	17.00	23	2.65	2.2 ± 0.6
	AFS	Kotz-21	Trachyandesite‡‡	5162.0	2.31	1	0.53	1	1.48	1	2.73	0.5
	EBB	Average††	Mg-andesite		1.10	7	1.16	8	5.03	8	2.65	0.7 ± 0.4
	EBB	Ob-G02	Mg-andesite	4184.0	1.63	1	1.72	1	6.94	1	2.73	1.1
	EBB	Ob-G03	Mg-andesite	4405.2	0.57	1	0.70	1	2.85	1	2.70	0.4
	EBB	Ob-G04	Mg-andesite	4411.3	0.29	1	0.96	1	2.99	1	2.65	0.5
	EBB	Ob-G05	Mg-andesite	4414.0	0.22	1	1.11	1	3.23	1	2.67	0.5
	EBB	Ob-G06	Mg-andesite	4546.5	1.13	1	1.19	1	5.20	1	2.80	0.8
	EBB	Ob-G07	Mg-andesite	4548.4	1.16	1	1.13	1	4.72	1	2.78	0.7
	EBB	1424††	Trachyandesite		2.37	1	3.36	1	14.40	1	2.65	2.0
	EBB	Grsk-50	Trachyandesite‡‡	4236.0	2.83	1	3.26	1	10.76	1	2.70	1.8
	EBB	Ob-G01	Trachyandesite‡‡	3770.4	1.65	1	1.29	1	5.64	1	2.66	0.9
	EBB	1408††	Trachyte		4.14	1	2.37	1	16.50	1	2.65	2.1
	MV	Grimmen1216††	Andesite		2.81	1	3.04	1	12.10	1	2.65	1.8
	MV/EBB	Gs-N03	Trachyandesite‡‡	4944.5	0.38	1	5.69	1	7.41	1	2.71	2.0
	Rügen	Gst-02	Andesite‡‡	1797.8	1.88	1	0.68	1	2.84	1	2.60	0.5
Rhyolitic	AFS	Average††	I‡		5.60	34	3.90	6	25.00	9	2.65	3.2 ± 0.5
rock	AFS	Average††	III‡		5.36	64	10.00	11	26.00	11	2.65	4.9 ± 0.7
	AFS	Average††	V‡		5.44	16	5.80	1	21.60	1	2.65	3.5
	AFS	Gp-01	III‡	4579.8	5.29	1	4.87	1	23.29	1	2.67	3.3
	AFS	Kotz-23	Va‡	5176.7	5.73	1	4.44	1	20.55	1	2.65	3.0
	AFS	Kotz-24	III‡	5427.1	3.47	1	6.56	1	23.70	1	2.69	3.6
	AFS	Kotz-25	III‡	5439.8	6.13	1	4.10	1	29.10	1	2.65	3.6
	AFS	Kotz-26	III‡,‡‡	5488.3	8.52	1	10.67	1	34.83	1	2.68	5.9
	AFS	Pes-02	I‡	3647.6	7.15	1	4.75	1	24.77	1	2.60	3.5
	AFS	Pes-03	I‡	3650.6	7.33	1	6.17	1	27.04	1	2.64	4.1
	AFS	R-32	I‡	4246.3	5.73	1	6.01	1	27.27	1	2.63	3.9
	AFS	R-34	I‡	4255.4	5.54	1	6.56	1	26.59	1	2.63	3.9
	AFS	R-36	I‡	4278.1	5.88	1	6.25	1	26.27	1	2.60	3.8
	AFS	Sw-01	IV‡	3723.6	6.44	1	5.20	1	17.69	1	2.64	3.1
	EBB	nn††	Rhyolite		5.01	1	4.58	1	19.00	1	2.65	2.9
	EBB	nn††	Rhyolite		5.50	1	3.43	1	11.70	1	2.65	2.2
	MV	Loss-N01	I‡	3177.3	5.23	1	4.70	1	25.76	1	2.56	3.3
	MV	nn††	Ia‡		3.24	1	4.61	1	22.50	1	2.65	3.0
	MV	Ba-04	II‡	3434.8	3.11	1	4.90	1	20.88	1	2.68	3.0
	MV	nn††	IIa‡		3.11	1	3.70	1	16.80	1	2.65	2.4
	MV	Fdln-N02	III‡	4597.4	4.68	1	7.00	1	26.63	1	2.61	3.9
	MV	Fdln-N03	III‡	4560.1	4.87	1	6.75	1	26.17	1	2.61	3.9
	MV	nn††	III‡		3.56	1	4.53	1	22.60	1	2.65	3.0
	MV/EBB	Gs-08	I‡	4771.1	6.28	1	3.67	1	26.87	1	2.63	3.3
	MV/EBB	Gs-N05	I‡	4813.2	5.79	1	3.98	1	27.23	1	2.64	3.4
	MV/EBB	Gs-N06	I‡	4766.7	5.72	1	4.72	1	26.74	1	2.66	3.5
	MV/EBB	Gs-U1	I‡	4774.8	6.09	1	4.06	1	28.02	1	2.66	3.5

Table 6. Continued.

Rock Type	Province**	Sample	Type	Depth (m)	K (%)	$N^{\dagger}$	U (ppm)	$N^{\dagger}$	Th (ppm)	$N^{\dagger}$	Density (10^3kg/m^3)	A (μW/m^3)
Rhyolitic	MV/EBB	Gs-U2	I‡	4815.0	5.97	1	3.17	1	28.31	1	2.67	3.3
rock	Rügen	Gst-N03	I‡	1524.5	4.92	1	5.43	1	21.63	1	2.71	3.4
	Rügen	Binz-01	III‡	1446.8	4.93	1	3.99	1	21.02	1	2.60	2.8
Granitic	AFS	Average††	Granite		4.22	2	10.00	1	14.00	1	2.65	4.0
rock	MV	Ba-12	Granopyhre	4685.0	3.91	1	5.56	1	26.04	1	2.65	3.5
	MV	Loissin1203††	Microgranite		3.86	1	4.04	1	19.10	1	2.65	2.7
	MV	Loss-N03	Microgranite	4315.9	2.56	1	6.80	1	24.84	1	2.63	3.6

*Determined for magmatic rocks by gamma spectroscopy and XRF/ICP-MS. Sample names of specimens investigated by gamma spectroscopy are underlined.
**Province designation after R. Benek (1995, personal communication): AFS = Altmark – Flechtingen – Subhercyn; EBB = East Brandenburg; MV = Mecklenburg – Vorpommern; see Figure 1.
†N = number of analyses.
††U, Th, and K data after R. Benek (1995, personal communication), densities estimated. Average = average value from Benek data.
‡Code name for rhyolitic rocks used by R. Benek (1995, personal communication).
‡‡Geochemical analysis allows no explicit determination; the samples Kotz-21 and Gst-02 are most probably altered andesites, and the sample Kotz-26 is most likely a strongly altered alkaline rhyolite.

Table 7. Radiogenic Heat Production (μW/m^3) of Rocks in the Different Magmatic Provinces

Permian – Carboniferous Magmatic Rocks		Basaltic Rocks Range		Mean**	$N^{\dagger}$	Andesitic Rocks Range		Mean**	$N^{\dagger}$	Method*
Province	AFS	0.3	0.9	0.7	4	0.5	2.8	1.8	3	A
								1.4	1	B
	EBB					0.4	2.1	1.0	11	A
						0.5	1.1	0.9	4	B
	MV					1.8	2.0	1.9	2	A
							0.5		1	B
	Rügen	<0.1	0.1	0.1	2		0.5		1	A
		0.3	0.6	0.4	3					B

		Rhyolitic Rocks Range		Mean**	$N^{\dagger}$	Granitic Rocks Range		Mean**	$N^{\dagger}$	Method*
Province	AFS	3.0	5.9	3.8	14		4.0		1	A
		2.1	4.0	3.4	7					B
	EBB	2.2	2.9	2.6	2					A
										B
	MV	2.4	3.9	3.3	12					A
		2.9	4.1	3.4	5					B
	Rügen	2.8	3.4	3.1	2	2.7	3.6	3.3	3	A
		3.0	3.1	3.0	2	1.8	3.0	2.9	3	B

*A = determined by laboratory measurements; B = determined by well-log analysis.
**Mean values are weighted averages.
†N = number of rock samples or gamma-ray sections used.

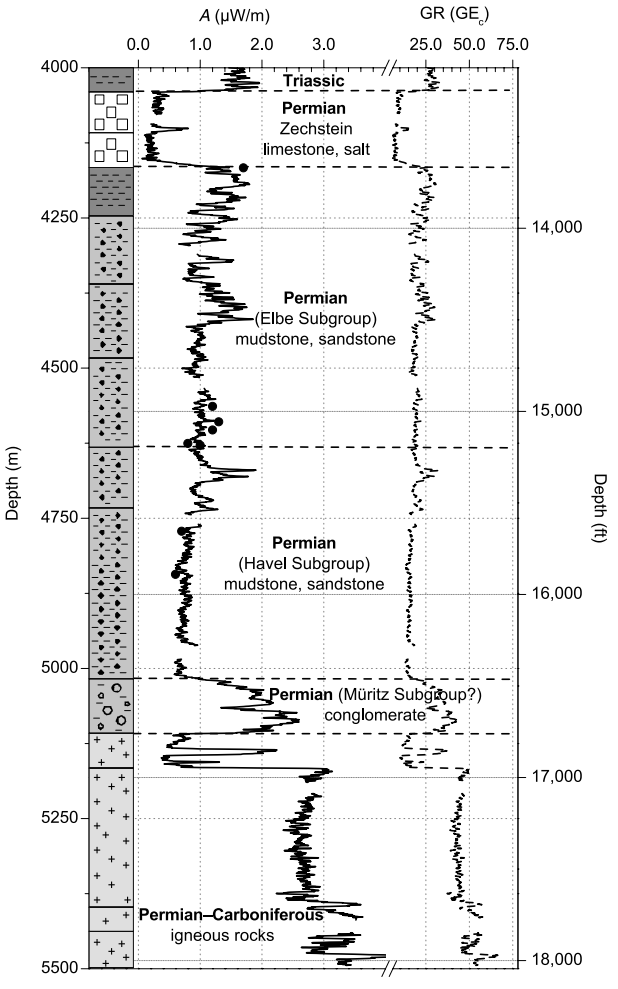

Figure 9. Heat production (*A*, solid line) determined for the Kotz 4/74 borehole using gamma-ray (GR) logging data (stippled line). Dots show heat-production values from laboratory measurements. Lithology and stratigraphy are denoted.

sediments (more fine-grained, commonly interbedded with organic-rich mudstone layers and coal seams) have a value of 2.0 $\mu W/m^3$.

Heat Budget of the Basin Fill

Figure 10 shows, for different parts of the NEGB, the heat budget provided by the basin fill. Summing up the increments of heat production in the different sedimentary formations multiplied by thickness, the super-Permian succession generates a heat flow that is variable in the basin. In areas where the succession is fairly thick, e.g., in the Pw 2/76 borehole (4000 m; 13,123 ft), the Gs 2/67 borehole (4077 m; 13,375 ft), and in the Gv 1/78 borehole (3827 m; 12,555 ft), it generates a heat flow of 4.0, 5.9, and 6.6 mW/m^2, respectively. At locations where the post-Permian succession is thin, which is over large salt diapirs and at the northern basin margin, this heat-flow component is low (e.g., RmwL 11A/69 [463 m; 1519 ft], 0.5 mW/m^2; Sam 101/62 [1400 m; 4593 ft], 1.8 mW/m^2, Figure 10A).

Because the heat flow in the NEGB was determined preferentially in Permian formations at depth of about 2500–6000 m (8200–19,600 ft) (Lotz, 2004), the heat-flow component by the post-Permian succession needs to be added to determine the surface heat flow sensu stricto. In the NEGB, this added component amounts to 8% at a maximum.

Variable composition and thickness of the different rock types are responsible for different heat budgets of the magmatic complexes. In the MV and Rügen area, the total thickness of the volcanic suite ranges from 200 m (660 ft) (western part) to about 2200 m (7200 ft) (southern Vorpommern). Rhyolitic

Table 8. Radiogenic Heat Production ($\mu W/m^3$) of Sedimentary Rocks

Stratigraphic Description		Mudstone-Siltstone				Sandstone				
		Range		Mean**	$N^\dagger$	Range		Mean**	$N^\dagger$	Method*
Rotliegende	Elbe Subgroup	2.2	2.7	2.5	2	0.7	1.2	1.0	5	A
		1.3	2.3	1.8	20	0.4	2.2	1.0	20	B
	Havel Subgroup	1.3	3.1	2.2	2	0.7	1.1	0.9	3	A
		1.7	2.2	1.9	9	0.6	1.6	1.1	13	B
	Müritz Subgroup		2.0		1					B
Carboniferous	Westphalian		2.7		1					A

*A = determined by laboratory analysis; B = determined by well-log analysis.
**Mean values are weighted averages.
$^\dagger N$ = number of rock samples or gamma-ray sections used.

Table 9. Formation Radiogenic Heat Production Determined by Log Analysis*

	Stratigraphic Description	Range ($\mu W/m^3$)		Mean** ($\mu W/m^3$)	*N*	Thickness (m)
Quaternary	Pleistocene	0.4	1.5	0.9	28	99
Tertiary	Neogene	0.7	1.4	1.0	16	95
	Paleogene	0.5	1.9	1.3	23	351
Cretaceous	Upper Cretaceous	0.3	0.9	0.6	22	417
	Lower Cretaceous	0.5	2.4	1.5	22	192
Jurassic	Malm	0.9	1.9	1.6	5	212
	Dogger	0.9	2.2	1.5	13	113
	Lias	0.9	2.0	1.5	23	289
Triassic	Keuper	0.7	2.1	1.6	27	413
	Muschelkalk	0.7	1.6	1.0	25	284
	Buntsandstein	1.0	2.5	1.8	26	796
	Zechstein	0.1	1.9	0.4	28	709
Permian	Elbe Subgroup	1.1	2.2	1.4	22	474
	Havel Subgroup	0.9	1.9	1.4	14	218
	Müritz Subgroup	2.0	2.5	2.1	2	146
	Altmark Subgroup†	1.1	1.8	1.5	4	33
Carboniferous	Stephanian†	1.5	2.3	1.7	8	227
	Westphalian	1.4	2.4	1.8	8	893
	Namurian	1.5	2.3	2.0	9	612
	Visean	0.9	2.1	1.4	5	660
	Tournaisian	0.7	1.7	0.9	3	387
Devonian	Famennian	0.8	1.4	1.2	2	48
	Frasnian	0.8	1.6	1.1	4	576
	Givetian	0.7	1.3	1.2	4	536
	Eifelian	1.0	1.5	1.4	2	481

*Thickness (m) and *N* are average thickness and number of log sections used.
**Means are weighted averages.
†Only sediments are regarded.

and ignimbritic rocks (about 90%) predominate over basaltic and andesitic rocks (about 5% each) in distribution and thickness. The heat budget of these rocks amounts to 0.6 mW/m^2 in the western part, up to 2 mW/m^2 in central Mecklenburg, 6.8 mW/m^2 at the FdlN 2/70 location (Figure 10B), and 7.5 mW/m^2 in southern Vorpommern. In the EBB complex, andesitic rocks (about 83%) predominate over rhyolitic rocks (about 17%), which also include volcanic rocks of dacite and trachyte composition. Thicknesses range between 200 and about 1500 m (660 and about 4900 ft). The estimated contribution to the regional heat flow ranges from 0.2 mW/m^2 in the southern EBB region to 1.5 mW/m^2 in the western EBB region (borehole Chi 1/71, Figure 10B). The AFS region, composed of rhyolitic rocks (about 67%), andesitic rocks (30%), and basaltic rocks (3%), accommodates a heat flow between 0.6 and 5 mW/m^2 in a 200–1700-m (660–5500-ft)-thick complex. For example, the 1.5-km (0.9-mi)-thick rhyolites in the Sw 2/64 borehole (Figure 10B) exhibiting a heat production of 3.5 $\mu W/m^3$ generate a heat flow at the upper bound of this range.

With the determination of radiogenic heat production in the NEGB, control on the heat budget is provided for a crustal segment that is up to 6 km (3.7 mi) thick. The heat flow generated in this segment is variable and amounts to about 8–14 mW/m^2.

DISCUSSION

Thermal Conductivity

Thermal conductivities ($\lambda_\perp$) of 4.0–4.2 W/m/K determined for Rotliegende sandstones are in contrast to previously published values of Permian sandstones

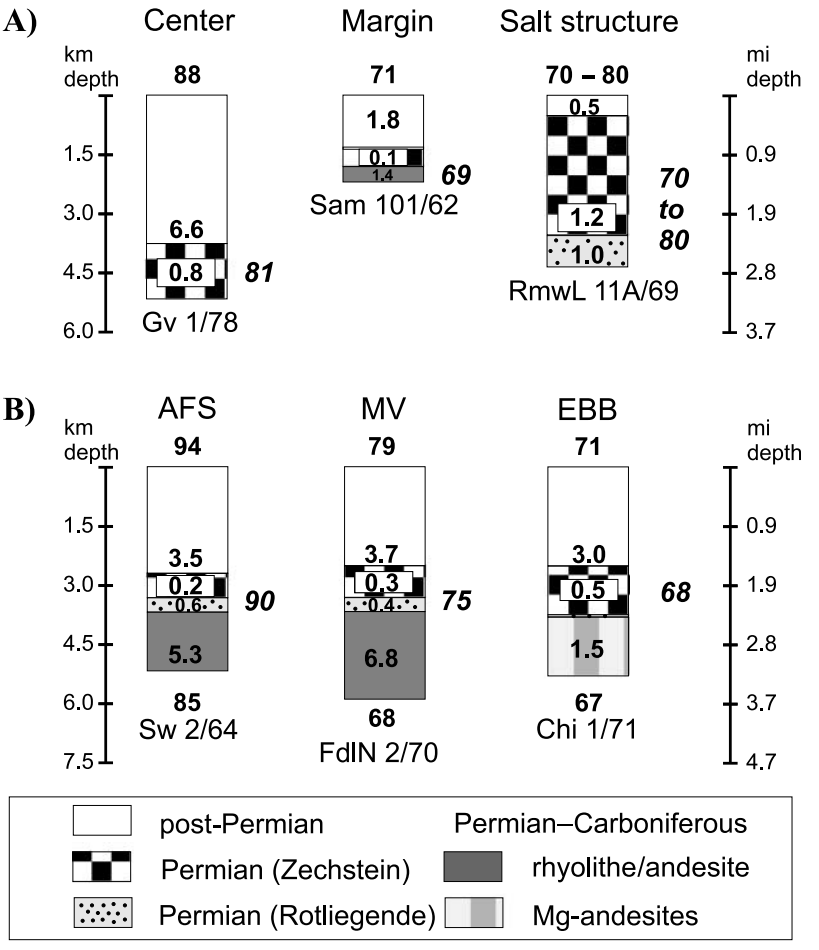

Figure 10. Heat budget of the basin fill for selected profiles of different stratigraphy and lithology. (A) Heat budget in the basin center, at the basin margin, and at salt structures. (B) Heat budget in areas of Permian–Carboniferous magmatic rocks. Numbers in italics denote the heat flow (plotted at depths of determination); numbers within columns denote the proportions of heat flow produced in each interval; numbers below columns refer to heat flow at that depth; and values above columns are the surface heat-flow values.

(2.7 W/m/K, n = 3, Becher and Meincke, 1968; 2.5 W/m/K, n = 82, Hurtig and Schlosser, 1976). In addition, the mean value for upper Carboniferous (roughly Pennsylvanian) sandstones of 4.7 W/m/K (n = 28, range 3.2–6.3 W/m/K) in this study is higher than the previously reported one (3.8 W/m/K, n = 13, Hurtig and Schlosser, 1976). One reason for the discrepancy is that the past lower values were measured under air-saturated conditions and not corrected for fluid saturation. Considering the value by Becher and Meincke (1968) of 2.7 W/m/K for dry sandstone and the mean porosity of 4% (this study) for Rotliegende sandstones, the water-saturated thermal conductivity would be on the order of 3.1 W/m/K. A value of 4.1 W/m/K (this study) could only be approached with a porosity of 13%. Unfortunately, sample porosity was not reported in the previous studies, so that the effects of different matrix porosity on bulk thermal conductivity could not be delineated. That different rock matrix composition is reflected in thermal-conductivity changes is shown in this study. For example, the thermal conductivity of Rotliegende samples from the Ob 1/68 borehole correlates with the quartz-grain content, the quartz-cement content, and other matrix minerals (such as illite). In addition, the thermal conductivity of quartz-rich samples decreases as the relative amount of phyllosilicates, carbonates, and feldspars increases. These changes are facies dependent. Thus, sample bias, not considering the different facies in the basin, may have been a reason why the previous thermal-conductivity values, especially for the Permian Rotliegende sandstones, were too low.

A discrepancy between measured and calculated thermal conductivity as observed in this study could also be delineated from the data published by Brigaud and Vasseur (1989). Although these authors noted a good agreement in the porosity range of 0–50%, there is a trend of measured water-saturated thermal conductivity being higher than the calculated value. At this point, it is difficult to assess any reason for the observed discrepancy between measured and calculated thermal-conductivity ratios. Pore-space geometry not reflected by the geometric-mean model may be responsible for this effect.

The thermal conductivity determined in this study is in marked contrast to values used in basinwide three-dimensional (3-D) models of the present-day temperature field of the NEGB (Bayer et al., 1997; Scheck, 1997). In these models, the lower values by Hurtig and Schlosser (1976) were applied, resulting in a thermal conductivity input of 1.8–2.4 W/m/K for the Permian Rotliegende and of 2.65 W/m/K (Scheck, 1997) for the pre-Permian sediments. In this study, for the Permian Rotliegende, values in the range of 3.2–3.7 W/m/K are reported, and for the pre-Permian rocks, values mostly greater than 3 W/m/K are reported. These higher values will significantly alter the thermal model of the NEGB by affecting the temperature gradient for a given heat flow. For example, using a heat flow of 60 mW/m^2, the in-situ temperature gradient in the Rotliegende interval (at about 5-km [3.14-mi] depth) would be reduced by about 11 °C/km using the new data. Permian–Carboniferous volcanic rocks in the previous 3-D thermal basin models comprise rhyolites and andesites, for which the same thermal conductivity of 2.5 W/m/K was used. This study shows that these rocks exhibit different values (2.9 W/m/K for rhyolites and 2.3 W/m/K for andesites). Moreover, petrological analysis of the igneous complexes in the NEGB has shown that additionally, trachyte (2.5 W/m/K), dacite (2.3 W/m/K), basalt (2.2 W/m/K), dolerite (2.0 W/m/K), and granitoid (3.1 W/m/K) are common. If one considers the mean rock composition of the different magmatic complexes according to Benek et al. (1996), the average thermal conductivity for the volcanic complexes would yield 2.7 W/m/K (AFS), 2.8 W/m/K (MV and Rügen), and 2.3 W/m/K (EBB), respectively. Future work is recommended to verify and fine tune the thermal model of the NEGB using the new data.

Radiogenic Heat Production

Analysis has shown that the Permian and post-Permian sediments of the NEGB have a heat production that is generally higher by 0.1–0.8 $\mu W/m^3$ than previously expected in 3-D basin modeling by Scheck (1997). The observed range of 0.4–1.8 $\mu W/m^3$ derived from well-log analysis of the post-Permian sediments is plausible considering that the post-Permian succession exhibits in parts large contents of claystone and shale. Heat production of Permian–Carboniferous magmatic rocks shows both higher values (rhyolitic and granitic rocks, 2.6–3.8 $\mu W/m^3$) and lower values (basaltic and andesitic rocks, 0.1–1.9 $\mu W/m^3$) compared to an undifferentiated value of 2.0 $\mu W/m^3$ used in the basin model by Scheck (1997). The new data of this study allow, for the first time, to differentiate the radiogenic heat production not only of rock types but also of igneous complexes.

Consequences for the Petroleum System of the NEGB

Carboniferous rocks are the main source rocks for hydrocarbon gases and nitrogen in the basin. Natural gases occur mainly in the Permian Rotliegende formations.

In thermal history and maturation studies, to assess hydrocarbon generation, the heat flow into a basin is an essential parameter. Unfortunately, at the time of recent investigation of methane and nitrogen generation and migration in the NEGB, the heat flow was only poorly constrained. Consequently, this parameter was treated instead as a guess in thermal subsidence and maturation modeling (Friberg, 2001). The new thermal data of this study allowed, for the first time, a specification of the present-day heat flow at particular borehole locations in the NEGB (Lotz, 2004; B. Norden, 2005, unpublished data). For example, in the depth interval of the Elbe Subgroup, a formation temperature gradient of 33 °C/km and a formation thermal conductivity of 3.2 W/m/K (corrected to 2.3 W/m/K for the in-situ conditions of 135 °C at 4200 m [13,700 ft]) result in a heat flow of 76 mW/m^2. Heat flow in the NEGB, determined in Permian formations at several kilometers depth, ranges from 64 to 90 mW/m^2. These values are higher than what was previously considered in thermal-history studies. For example, for the island of Rügen, where a present-day heat flow of about 70 mW/m^2 results from new data, work by Friberg (2001) provided a thermal-maturation history that was adjusted to a very low present-day heat flow of 43 mW/m^2. Similar to this, a discrepancy was observed in the Barth 1/63 borehole and along a 2-D cross section through the basin, where a present-day heat flow of 58 and of 52–55 mW/m^2, respectively, was considered. In all models, the heat flow was lowered toward the present-day value from a value of 70–77 mW/m^2 during the time of maximum subsidence (in the Permian) to fit measured vitrinite reflectance data in this borehole. The higher present-day basement heat flow in the NEGB than originally considered suggests that the existing thermal-history models in the NEGB should be revisited. The new data indicate a thermal input from the basement into the sedimentary basin fill that must have been larger over longer time in basin history than previously assumed.

The subsidence and thermal-maturation modeling (Friberg, 2001) was based on using the program code

PETROMod. The program accommodates the computation of a porosity-dependent bulk thermal conductivity based on standard matrix thermal conductivity for each rock type. Values for the Permian Rotliegende formations differ from the values that are now available from laboratory measurements. For example, the program would calculate for the Havel Subgroup (with a sediment porosity of 3%, this study) a bulk thermal conductivity (at 20°C, water saturated) on the order of 2.5–3.0 W/m/K and, for the Elbe Formation, on the order of 2.2 W/m/K, respectively, which is much lower than those determined in the laboratory (3.7 and 3.2 W/m/K). In addition, the PETROMod calculations show for these subgroups a higher present-day porosity of 9–16%.

To quantify the possible effects of different thermal conductivity on the paleogeothermal conditions, a case study was conducted at the Gv 1/78 borehole (Figure 4) located in the northwestern part of the NEGB, in the basin area of maximal subsidence in the Permian. The subsidence is reconstructed by backstripping the present sediment thickness of Carboniferous Namurian to Quaternary units using porosity-dependent decompaction at time steps of 1 m.y. Paleotemperature and vitrinite reflectance are simultaneously calculated as a function of time and depth in a heat conduction regime as described by Förster et al. (1998). Thermal conductivity is corrected for temperature. Two different thermal-conductivity scenarios are modeled for upper Paleozoic units that comprise more than 50% of the entire succession. Scenario I is according to values used in the 3-D basin model by Scheck (1997), and scenario II is based on data of this study. The differences in matrix thermal conductivity are 1.4 W/m/K for the Elbe Subgroup, 1.6 W/m/K for the Havel Subgroup, 0.3 W/m/K for the Permian–Carboniferous volcanic rocks, and 0.9–1.4 W/m/K for the Carboniferous (Namurian to Stephanian) formations. In both scenarios, radiogenic heat production from this study is considered. The boundary condition of the model (temperature at 100 km [62 mi] depth) and the starting condition of surface heat flow in the two scenarios are the same.

Results of modeling show for the Permian Rotliegende formations at 4900–7200-m (16,076–23,600-ft) depth present-day temperatures that differ by 13–25°C. The degree of present-day thermal maturation is 0.3–0.4 EASY % R_o (vitrinite reflectance after Sweeny and Burnham, 1990) in scenario I and 1.1–2.7 EASY % R_o in scenario II. Although the model is not fine tuned, this level of maturation already corroborates vitrinite reflectance measured in this part of the NEGB (Hoth, 1997).

A neglect of radiogenic heat production in the sedimentary succession in the Gv 1/78 model results in a paleogeothermal field that allows for less thermal maturation of organic matter in the Permian Rotliegende. Present-day temperatures would decrease by 32–47°C, the 120°C isotherm would be 1450 m (4757 ft) deeper, and the present-day thermal maturation would be lower by 0.4–1.2%. In addition, thermal maturation is accommodated later in time (e.g., by 18 m.y. for 1.3 EASY % R_o).

SUMMARY

From this study, a set of thermal data is now available that is important for geothermal and hydrocarbon studies in the NEGB. Thermal conductivity measured on core samples is higher than previously expected for the upper Paleozoic. It would be of interest for future investigations whether fresh core samples and complete core records from recent boreholes will differ from these data. Radiogenic heat production was determined both by laboratory measurements and by well-log analysis. Old gamma-ray well logs (in GE-reading) proved usable for the determination of radiogenic heat production after being converted into modern API units by the employment of an empiric correction equation.

Both the thermal conductivity and the radiogenic heat production in basin sediments and magmatic rocks display a larger variability than previously shown and used in basin modeling approaches. This variability also is spatially related. Thus, if thermal properties are summarized or averaged for sedimentary formations and igneous complexes, their specific properties (facies and composition) have to be considered. Assessment of the internal heat of a basin is important for evaluating the surface heat flow sensu stricto and the heat flow used as input into basin modeling approaches. In the NEGB, the basin fill comprising sedimentary and igneous rocks contributes up to 8–14 mW/m^2 to surface heat flow. Consideration of the new data on thermal conductivity and heat production brings new aspects to hydrocarbon and geothermal resource evaluation for the NEGB.

REFERENCES CITED

Anonymous, 1974, Recommended practice for standard calibration and form for nuclear logs: American Petroleum Institute, API RP-33, 13 p.

Baisert, D., 1990, Zeitliche Fixierung diagenetischer Prozesse in Saxon-Sandsteinen der DDR (in German): Zeitschrift Angewandte Geologie, v. 36, p. 253–256.

Bayer, U., M. Scheck, and M. Koehler, 1997, Modeling of the 3D thermal field in the Northeast German Basin: Geologische Rundschau, v. 86, p. 241–251.

Becher, D., and W. Meincke, 1968, Wärmefluss zwischen Harz und Prignitz (in German): Zeitschrift Angewandte Geologie, v. 14, p. 291–297.

Benek, R., W. Kramer, T. McCann, M. Scheck, J. Negendank, D. Korich, H.-D. Huebscher, and U. Bayer, 1996, Permo-Carboniferous magmatism of the Northeast German Basin: Tectonophysics, v. 266, p. 379–404.

Blackwell, D. D., and J. L. Steele, 1989, Thermal conductivity of sedimentary rocks: Measurement and significance, *in* N. D. Naeser and T. H. McCulloh, eds., Thermal history of sedimentary basins: New York, Springer-Verlag, p. 13–36.

Brigaud, F., and G. Vasseur, 1989, Mineralogy, porosity and fluid control on thermal conductivity of sedimentary rocks: Geophysical Journal, v. 98, p. 525–542.

Bücker, C., and L. Rybach, 1996, A simple method to determine heat production from gamma-ray logs: Marine and Petroleum Geology, v. 13, no. 4, p. 373–377.

Čermák, V., H.-G. Huckenholz, L. Rybach, R. Schmid, J. R. Schopper, M. Schuch, D. Stöffler, and J. Wohlenberg, 1982, Physical properties of rocks, v. 1, subvolume A, *in* G. Angenheister, ed., Landolt-Börnstein, New Series, V/1a, Geophysics and Space Research: Heidelberg, Germany, Springer, p. 1–373.

Deming, D., J. A. Nunn, S. Jones, and D. S. Chapman, 1990, Some problems in thermal history studies, *in* V. N. Nuccio and C. E. Barker, eds., Applications of thermal maturity studies to energy exploration: Rocky Mountain Section, SEPM, p. 61–80.

Dulski, P., 2001, Reference materials for geochemical studies: New analytical data by ICP-MS and critical discussion of reference values: Journal of Geostandards and Geoanalysis, v. 25, p. 87–125.

Förster, A., 2001, Analysis of borehole temperature data in the Northeast German Basin: Continuous logs versus bottom-hole temperatures: Petroleum Geoscience, v. 7, p. 241–254.

Förster, A., D. F. Merriam, and P. Hoth, 1998, Geohistory and thermal maturation in the Cherokee Basin (mid-continent, U.S.A.): Results from modeling: AAPG Bulletin, v. 82, no. 9, p. 1673–1693.

Franke, D., 1990, Der präpermische Untergrund der Mitteleuropäischen Senke-Fakten und Hypothesen (in German): Niedersächsische Akademie der Geowissenschaften Veröffentlichungen, v. 4, p. 19–75.

Franke, D., N. Hoffmann, and W. Lindert, 1996, The Variscan deformation front in East Germany: Part 2— Tectonic interpretation: Zeitschrift Angewandte Geologie, v. 42, p. 44–56.

Friberg, L., 2001, Untersuchungen zur Temperatur- und Absenkungsgeschichte sowie zur Bildung und Migration von Methan und molekularem Stickstoff im Nordostdeutschen Becken (in German): Berichte des Forschungszentrums Jülich, Jül-3914, Jülich, Germany, Forschungszentrum Jülich GmbH, 248 p.

Gast, R., M. Pasternak, J. Piske, and H.-J. Rasch, 1998, Das Rotliegend im nordostdeutschen Raum: Regionale Übersicht, Stratigraphie, Fazies und Diagenese (in German): Geologisches Jahrbuch, v. 149, p. 59–79.

Gebhardt, U., H. Helmuth, O. Kleditzsch, and S. Süssmuth, 1995, Havel-Subgruppe, Stratigraphie von Deutschland I (in German), *in* E. Plein, ed., Stratigraphie von Deutschland I: Norddeutsches Rotliegendbecken, Rotliegend-Monographie Teil II, Courier Forschungsinstitut Senckenberg, Frankfurt a. M., v. 183, p. 110–117.

German Stratigraphic Commission, ed., 2002, Stratigraphic table of Germany 2002.

Glennie, K. W., 1998, Lower Permian— Rotliegend, *in* K. W. Glennie, ed., Petroleum geology of the North Sea: Basic concepts and recent advances: Oxford, Blackwell, p. 137–173.

Hartmann, A., V. Rath, and C. Clauser, 2005, Thermal conductivity from core and well log data: International Journal of Rock Mechanics and Mining Sciences, v. 42, p. 1042–1055.

Hoth, K., J. Rusbült, K. Zagora, H. Beer, and O. Hartmann, 1993, Die tiefen Bohrungen im Zentralabschnitt der Mitteleuropäischen Senke— Dokumentation für den Zeitabschnitt 1962–1990 (in German): Gesellschaft für Geowissenschaften, Schriftenreihe Geowissenschaften, v. 2, 145 p.

Hoth, P., 1997, Fazies und Diagenese von Präperm-Sedimenten der Geotraverse Harz-Rügen (in German): Gesellschaft für Geowissenschaften, Schriftenreihe Geowissenschaften, v. 4, 139 p.

Hurtig, E., and P. Schlosser, 1976, Geothermal studies in the GDR and relations to the geological structure, *in* A. Adam, ed., Geoelectric and geothermal studies (east-central Europe, Soviet Asia): Budapest, Committee of the Academies of Sciences of Socialist Countries for Planetary Geophysical Investigation (KAPG) Geophysical Monograph, Akademiai Kiado, p. 384–394.

Katzung, G., U. Fischer, W.-D. Sigeneger, K.-H. John, S. Süssmuth, and D. Warncke, 1977, Die Saxongliederung im Zentralabschnitt der Mitteleuropäischen Senke: Zeitschrift Angewandte Geologie, v. 23, p. 559–561.

Lewis, T., H. Villinger, and E. Davis, 1993, Thermal conductivity measurement of rock fragments using a pulsed needle probe: Canadian Journal of Earth Sciences, v. 30, p. 480–485.

Lokhorst, A., ed., 1998, NW European gas atlas: Haarlem, Nederlands Institute voor Toegepaste Geowetenschappen TNO, CD-ROM.

Lotz, B., 2004, Neubewertung des rezenten Wärmestroms im Nordostdeutschen Becken (in German): Scientific Technical Report STR 04/04, Potsdam, Germany, GeoForschungsZentrum Potsdam, 226 p.

Plein, E. , ed., 1995, Stratigraphie von Deutschland I (in German): Norddeutsches Rotliegendbecken, Rotliegend-Monographie Teil II, Courier Forschungsinstitut Senckenberg, Frankfurt a. M., v. 183, 193 p.

Popov, Y. A., D. F. C. Pribnow, J. H. Sass, C. F. Williams, and H. Burkhardt, 1999, Characterization of rock thermal conductivity by high-resolution optical scanning: Geothermics, v. 28, p. 253–276.

Popov, Y. A., V. Tertychnyi, R. Romushkevich, D. Korobkov, and J. Pohl, 2003, Interrelations between thermal conductivity and other physical properties of rocks: Experimental data: Pure and Applied Geophysics, v. 160, p. 1137–1161.

Pribnow, D., and J. H. Sass, 1995, Determination of thermal conductivity from deep boreholes: Journal of Geophysical Research, v. 100, p. 9981–9994.

Rieke, H., 2001, Sedimentologie, Faziesarchitektur und Faziesentwicklung des kontinentalen Rotliegenden im Norddeutschen Becken (NEDB) (in German): Scientific Technical Report STR 01/14, Potsdam, Germany, GeoForschungsZentrum Potsdam, 138 p.

Rybach, L., 1976, Die Gesteinsradioaktivität und ihr Einfluss auf das Temperaturfeld in der kontinentalen Kruste (in German): Zeitschrift für Geophysik, v. 42, no. 2, p. 93–101.

Scheck, M., 1997, Dreidimensionale Strukturmodellierung des Nordostdeutschen Beckens unter Einbeziehung von Krustenmodellen (in German): Scientific Technical Report STR 97/10, Potsdam, Germany, GeoForschungsZentrum Potsdam, 126 p.

Scheck, M., and U. Bayer, 1999, Evolution of the Northeast German

Basin— Inferences from a 3D structural model and subsidence analysis: Tectonophysics, v. 313, p. 145–169.
Schmidt Mumm, A., and M. Wolfgramm, 2002, Diagenesis and fluid mobilisation during the evolution of the North German Basin— Evidence from fluid inclusion and sulphur isotope analysis: Marine and Petroleum Geology, v. 19, p. 229–246.
Schön, J. H., 1996, Physical properties of rocks: Fundamentals and principles of petrophysics, *in* K. Helbig and S. Teitel, eds., Handbook of geophysical exploration: Section 1. Seismic exploration: Oxford, United Kingdom, Pergamon, v. 18, 583 p.
Sweeny, J. J., and A. K. Burnham, 1990, Evaluation of a simple model of vitrinite reflectance based on chemical kinetics: AAPG Bulletin, v. 74, no. 10, p. 1559–1570.
Woodside, W., and J. Messmer, 1961a, Thermal conductivity of porous media: I. Unconsolidated sands: Journal of Applied Physics, v. 32, p. 1688–1699.
Woodside, W., and J. Messmer, 1961b, Thermal conductivity of porous media: II. Consolidated sands: Journal of Applied Physics, v. 32, p. 1699–1706.
Ziegler, P. A., 1990, Geological atlas of Western and Central Europe: The Hague, Shell International Petroleum Maatschappij, 239 p. and 56 enclosures.